AGU ADVANCING EARTH AND SPACE SCIENCES

Earth and Space Science

RESEARCH ARTICLE
10.1029/2023EA003279

Observed Global Changes in Sector-Relevant Climate Extremes Indices—An Extension to HadEX3

Robert J. H. Dunn[1], Nicholas Herold[2], Lisa V. Alexander[3,4], Markus G. Donat[5,6], Rob Allan[7], Margot Bador[8], Manola Brunet[9], Vincent Cheng[10], Wan Maisarah Wan Ibadullah[11], Muhammad Khairul Izzat Bin Ibrahim[12], Andries Kruger[13,14], Hisayuki Kubota[15], Tanya J. R. Lippmann[16], Jose Marengo[17], Sifiso Mbatha[13], Simon McGree[18], Sandile Ngwenya[13], Jose Daniel Pabon Caicedo[19], Andrea Ramos[20,21], Jim Salinger[22], Gerard van der Schrier[23], Arvind Srivastava[24], Blair Trewin[18], Ricardo Vásquez Yáñez[25], Jorge Vazquez-Aguirre[26], Claudia Villaroel Jiménez[25], Russ Vose[27], Mohd Noor'Arifin Bin Hj Yussof[12], and Xuebin Zhang[28]

[1]Met Office Hadley Centre, Exeter, UK, [2]Applied Climate Science Ptd Ltd., Adelaide, SA, Australia, [3]Climate Change Research Centre, UNSW Sydney, Kensington, NSW, Australia, [4]ARC Centre of Excellence for Climate Extremes, UNSW Sydney, Kensington, NSW, Australia, [5]Barcelona Supercomputing Center, Barcelona, Spain, [6]Catalan Institution for Research and Advanced Studies (ICREA), Barcelona, Spain, [7]Centre for Maritime Historical Studies, University of Exeter, Exeter, UK, [8]CECI Université de Toulouse, CERFACS/CNRS, Toulouse, France, [9]Department of Geography, Centre for Climate Change, University Rovira I Virgili, Tarragona, Spain, [10]Climate Research Division, Environment and Climate Change Canada, Toronto, ON, Canada, [11]Malaysian Meteorological Department, Kuala Lumpur, Malaysia, [12]Brunei Darussalam Meteorological Department, Ministry of Transport and Infocommunications, Brunei, Brunei Darussalam, [13]Climate Service, South African Weather Service, Pretoria, South Africa, [14]Department of Geography, Geoinformatics and Meteorology, Faculty of Natural and Agricultural Sciences, University of Pretoria, Pretoria, South Africa, [15]Department of Earth and Planetary Sciences, Hokkaido University, Sapporo, Japan, [16]Department of Earth Sciences, Vrije Universiteit Amsterdam, Amsterdam, The Netherlands, [17]National Center for Monitoring and Early Warning of Natural Disasters CEMADEN, Sao Paulo, Brazil, [18]The Bureau of Meteorology, Melbourne, VIC, Australia, [19]Departamento de Geografía, Universidad Nacional de Colombia, Bogotá, Colombia, [20]Instituto Nacional de Meteorologia—INMET, Brasília, Brazil, [21]Fundação de Desenvolvimento Científico e Cultural, Lavras, Brazil, [22]School of Geography, Environmental and Earth Sciences, Victoria University of Wellington, Wellington, New Zealand, [23]Royal Netherlands Meteorological Institute, De Bilt, The Netherlands, [24]Climate Research and Services, IMD Pune, Pune, India, [25]Dirección Meteorológica de Chile, Santiago, Chile, [26]WMO Expert Team on Climate Information for Decision-Making (ET-CID), Xalapa, Mexico, [27]NOAA/NCEI, Asheville, NC, USA, [28]Pacific Climate Impacts Consortium, University of Victoria, Victoria, BC, Canada

Abstract Global gridded data sets of observed extremes indices underpin assessments of changes in climate extremes. However, similar efforts to enable the assessment of indices relevant to different sectors of society have been missing. Here we present a data set of sector-specific indices, based on daily station data, that extends the HadEX3 data set of climate extremes indices. These additional indices, which can be used singly or in combinations, have been recommended by the World Meteorological Organization and are intended to empower decision makers in different sectors with accurate historical information about how sector-relevant measures of the climate are changing, especially in regions where in situ daily temperature and rainfall data are hard to come by. The annual and/or monthly indices have been interpolated on to a 1.875° × 1.25° longitude-latitude grid for 1901–2018. We show changes in globally-averaged time series of these indices in comparison with reanalysis products. Changes in temperature-based indices are consistent with global scale warming, with days with $T_{max} > 30$°C (TXge30) increasing virtually everywhere with potential impacts on crop fertility. At the other end of the scale, the number of days with $T_{min} < -2$°C (TNltm2) are reducing, decreasing potential damage from frosts. Changes in heat wave characteristics show increases in the number, duration and intensity of these extreme events in most places. The gridded netCDF files and, where possible, the underlying station indices are available from https://www.metoffice.gov.uk/hadobs/hadex3 and https://www.climdex.org.

Plain Language Summary To be able to assess changes in extreme temperature and rainfall events across the globe, data sets which capture characteristics of these extreme events are required. The use of indices for these characteristics further enables both data sharing and the comparison of events across the world. Extreme events have impacts across human health, our infrastructure and the natural environment. So far there has not been a global product which presents indices which are relevant for different sectors of our society,

Key Points:

- We present a sector specific extension to a data set of gridded temperature and precipitation extremes
- This first quasi-global product of these indices will support decision makers in a wide range of sectors
- Long-term changes show increases in intensity, frequency, and duration of warm extremes, and corresponding decreases in cool extremes

Supporting Information:

Supporting Information may be found in the online version of this article.

Correspondence to:

R. J. H. Dunn,
robert.dunn@metoffice.gov.uk

Citation:

Dunn, R. J. H., Herold, N., Alexander, L. V., Donat, M. G., Allan, R., Bador, M., et al. (2024). Observed global changes in sector-relevant climate extremes indices—An extension to HadEX3. *Earth and Space Science*, *11*, e2023EA003279. https://doi.org/10.1029/2023EA003279

Received 7 SEP 2023
Accepted 15 JAN 2024

Author Contributions:

Conceptualization: Robert J. H. Dunn, Lisa V. Alexander, Markus G. Donat
Data curation: Robert J. H. Dunn
Formal analysis: Robert J. H. Dunn
Investigation: Robert J. H. Dunn

Methodology: Robert J. H. Dunn, Nicholas Herold, Lisa V. Alexander, Markus G. Donat, Margot Bador, Tanya J. R. Lippmann
Resources: Rob Allan, Manola Brunet, Vincent Cheng, Wan Maisarah Wan Ibadullah, Muhammad Khairul Izzat Bin Ibrahim, Andries Kruger, Hisayuki Kubota, Tanya J. R. Lippmann, Jose Marengo, Sifiso Mbatha, Simon McGree, Sandile Ngwenya, Jose Daniel Pabon Caicedo, Andrea Ramos, Jim Salinger, Gerard van der Schrier, Arvind Srivastava, Blair Trewin, Ricardo Vásquez Yáñez, Jorge Vazquez-Aguirre, Claudia Villaroel Jiménez, Russ Vose, Mohd Noor'Arifin Bin Hj Yussof, Xuebin Zhang
Software: Robert J. H. Dunn, Nicholas Herold, Lisa V. Alexander
Validation: Robert J. H. Dunn
Visualization: Robert J. H. Dunn
Writing – original draft: Robert J. H. Dunn
Writing – review & editing: Robert J. H. Dunn, Nicholas Herold, Lisa V. Alexander, Markus G. Donat, Xuebin Zhang

including health, agriculture and water resources. In this work we present an extension to an existing data set of extremes indices, HadEX3, by including indices defined by the World Meteorological Organization which were developed with sector specific applications in mind. We have used the same approach and methodology, and where possible the same underlying daily temperature and rainfall observations. The temperature indices show changes consistent with global scale warming, with heat wave characteristics showing increases in the number, duration and intensity of these extreme events in most places. The data files are available for use by interested researchers in their work.

1. Introduction

The study of global land-surface climate extremes based on in situ observations has been accomplished through the use of a number of climate indices. The foremost set of these indices was developed by the former World Meteorological Organization (WMO)/World Climate Research Programme/Joint WMO-IOC (UNESCO's Intergovernmental Oceanographic Commission) Technical Commission for Oceanography and Marine Meteorology (JCOMM) Expert Team on Climate Change Detection and Indices (ETCCDI). Using standard climate extremes indices based on daily data allowed the derived products to be widely and easily shared, as in many cases the daily observations are not freely available (Alexander et al., 2019; Thorne et al., 2017; Zhang et al., 2011). To further increase the amount of available data, workshops were organized where these indices were calculated from the data provided by attendees (e.g., Donat et al., 2014; Meteorological Service Singapore, 2019), and standardized software was developed to allow the widest possible set of contributors (e.g., RClimdex, Climpact). The existence and support of standardized software enabled the development of global gridded data sets of climate extremes which combined input data from a wide range of input sources, with contributions from institutions around the world—HadEX (Alexander et al., 2006), HadEX2 (Donat et al., 2013b), HadEX3 (Dunn et al., 2020), and GHCNDEX (Donat et al., 2013a)—along with a multitude of regional and national studies which are intercomparable by virtue of the standard approach. These have been the basis for assessment of how observed temperature and precipitation extremes are changing globally.

However, the "ETCCDI indices" were initially developed for detection and attribution, and the monitoring of land surface extremes from a climate science perspective. The valuable approach of developing indices, running workshops and providing standardized software was adopted by the WMO Commission for Climatology (CCl) Expert Team on Climate Risk and Sector-specific Climate Indices (ET-CRSCI) and subsequently the Expert Team for Sector-specific Climate Indices (ET-SCI) to develop the ability to monitor changes in climate conditions relevant to a number of societal sectors (Alexander & Herold, 2015; Herold & Alexander, 2016). These "ET-SCI indices" extend the ETCCDI indices and enable those working in sectors such as agriculture, health and water resources to more directly determine how relevant climate extremes affect their focal regions, using both single and multiple variable indices to identify simple and complex climate risks for example, (Herold et al., 2018; McGree et al., 2020; Nakaegawa & Murazaki, 2022; Oliveira et al., 2022; Wang et al., 2023). Since the inaugural workshop in 2011 held to develop these indices with experts in these fields, they have continued to be discussed, assessed and updated to ensure their relevance through regional workshops and WMO-related group discussions. The combined set of indices developed by both the ETCCDI and ET-SCI are termed the "Climpact indices." Indices defined by both Expert Teams are applicable across different sectors, and currently fall under the WMO Expert Team on Climate Information for Decision-Making (ET-CID).

In this manuscript we present an extension to the HadEX3 data set which includes the additional indices from the Climpact set. The new indices are presented in Section 2, and updates to the data in Section 3. We give a brief summary of the methods highlighting the differences to HadEX3 in Section 4, as well as a validation of new input data over China in Section 5. Some high-level results are presented in Section 6 and we summarize in Section 7.

2. Indices

We have calculated the additional Climpact indices which were not originally included in HadEX3 (Dunn et al., 2020). As with the original extremes indices, these sector-specific indices are based on daily observations of precipitation accumulations, and maximum and minimum temperature. The complete set of Climpact indices were developed with the following sectors in mind: Health, Agriculture and Food Security, and Water Resources; and so extend the applicability of the ETCCDI indices for these sectors. These indices may also be useful in other

sectors, for example, Disaster Risk Reduction, Energy or Forestry. We outline the new indices in the Climpact set in Tables 1–3. Examples of their application to different sectors can be found at www.climdex.org/learn/indices/sector and in Herold et al. (2018) and McGree et al. (2020).

A number of the temperature indices expand the set using fixed temperature thresholds from the ETCCDI (ID ["TXlt0"], FD ["TNlt0"], TR ["TNgt20"], SU ["TXgt25"]). These new threshold values were chosen for their sector relevance during the workshops held to develop the indices. For example, TNlt2 can be used in situations when ground cools faster than the air, and so the 2 m screen temperature is greater than the surface temperature. Hence this index captures instances of grass or ground frost, whereas the pre-existing FD captures air frost. The next threshold, TNltm2, captures hard-freeze events of significant frost. Both these indices are therefore relevant for agriculture given the impact of frost events on certain crops.

A number of the indices allow for user-defined values (CDDcold*n*, HDDheat*n*, GDDgrow*n*, CSDI*d*, WSDI*d*, TX*d*TN*d*, TXb*d*TNb*d*, Rx*d*day, *M*month_SPI, and *M*month_SPEI, see Table 1 for definitions). For users of these indices who are making their own calculations, this allows for flexibility in producing indices which are more regionally relevant. For the heating degree days (HDDheat*n*, Quayle & Diaz, 1980; H. C. S. Thom, 1954), a base temperature of 18°C (~65°F) is commonly used in the USA (https://www.weather.gov/key/climate_heat_cool), whereas lower temperatures are used in some parts of Europe (15.5°C by the UK Met Office, Spinoni et al., 2018). Cooling degree days (CDDcold*n*, De Rosa et al., 2014; E. C. Thom, 1959) in the USA also uses 18°C, but higher temperatures are used in other locations (22°C by the UK Met Office, Spinoni et al., 2018). Growing degree days (GDDgrow*n*, Ferchault de Réaumur, 1735) are important for crops and pests where temperatures limit development, and are specific for each species. Cereals (wheat, barley, rye, oats) have a base temperature around 5°C, whereas maize, rice, soy around 10°C.

For this global product it is necessary that we use a single value for each of these indices so that the stations can be combined. Therefore, we have chosen values which allowed for the greatest number of user contributed indices from stations to be included in the final product (CDDcold18, HDDheat18, GDDgrow10, CSDI3, WSDI3, TX2TN2, TXb2TNb2, Rx3day, 24month_SPI, and 24month_SPEI), so that the behavior of these indices can be assessed over a large area.

We note that in doing so, the values chosen may not be the most appropriate for all locations or applications. Along with the data set presented in this manuscript, we herein also publicize these indices for calculation by others. And hence, we strongly encourage those using and calculating their own versions of these indices to think about what the most appropriate user-defined values are for their application.

In this collection of sector specific indices there are a number which characterize heat waves and cold waves. In addition to the warm spell and cold spell duration indices (WSDI*d*, CSDI*d*), a number of heat wave characteristics have been defined by Perkins and Alexander (2013), see Table 2. These measures are calculated for heat waves and cold waves which have been identified using a variety of separate metrics, outlined in Table 3. Each of the measures in Table 2 is calculated using each of the definitions in Table 3, overall resulting in 20 indices characterizing heat waves and cold waves.

The heat wave definitions in Table 3 use thresholds calculated from the quantities shown. For the TN90 and TX90 thresholds, the 90th percentile thresholds are determined for each calendar day using the chosen reference period (1981–2010), and result in a smoothly varying threshold throughout the year. The Excess Heat Factor (EHF), and conversely the Excess Cold Factor (ECF), were defined by Nairn and Fawcett (2015) for Australian use, but have gained popularity globally as an effective measure of health impacts from heat (Nairn et al., 2018). It is the combination of two indices based on the daily average temperature (mean of T_{max} and T_{min}). One accounts for acclimatization by comparing the temperature anomaly over a 3-day window against the preceding 30 days, and the other accounts for long term change by comparing the anomaly of the 3-day window against the climatological 90th percentile of the average daily temperature, using the "PA13" setting in Climpact2. The TN90 and TX90 heat wave indices are only calculated for the summer season (November-March for the Southern Hemisphere, May-September for the Northern Hemisphere), and we note that this may limit their use in some tropical and subtropical climates. The Excess Heat Factor and Excess Cold Factors are calculated over the entire calendar year. For further details on the EHF and ECF see Nairn and Fawcett (2015), Perkins & Alexander, 2013, Herold and Alexander (2016).

Earth and Space Science
10.1029/2023EA003279

Table 1
Details of the ET-SCI Indices and the Numbers of Stations Available for Each One That Were Taken Forward Into the Gridded Product After Selection for Record Length and Quality Control

Index	Name	Description	Units	Sector(s)	Stations (1981–2010 ref. Period)
CDDcold*n*	Cooling degree days	The annual sum of $T_{mean} - n$, where n is a user defined temperature and $T_{mean} > n$	degree-days	H	5,530
HDDheat*n*	Heating degree days	The annual sum of $n - T_{mean}$, where n is a user defined temperature and $T_{mean} < n$	degree-days	H	5,529
GDDgrow*n*	Growing degree days	The annual sum of $T_{mean} - n$, where n is a user defined temperature and $T_{mean} > n$	degree-days	H, A	5,534
CSDI*d*	User defined CSDI	Cold spell duration index, annual count of days where d or more con secutive days experience T_{max} < 10th percentile	days	H, A, W	5,647
WSDI*d*	User defined WSDI	Warm spell duration index, annual count of days where d or more con secutive days experience T_{max} > 90th percentile	days	H, A, W	5,681
TNlt2	T_{min} below 2°C	Number of days when T_{min} < 2°C	days	A	5,751
TNltm2	T_{min} below −2°C	Number of days when T_{min} < −2°C	days	A	5,751
TNltm20	T_{min} below −20°C	Number of days when T_{min} < −20°C	days	H, A	5,751
TXge30	T_{max} at least 30°C	Number of days when $T_{max} \geq$ 30°C	days	H, A	5,790
TXge35	T_{max} at least 35°C	Number of days when $T_{max} \geq$ 35°C	days	H, A	5,790
TNm	Mean T_{min}	Mean daily minimum temperature	°C		5,730
TXm	Mean T_{max}	Mean daily maximum temperature	°C		5,771
TMm	Mean T_{mean}	Mean daily mean temperature	°C		5,582
TMlt10	T_{mean} below 10°C	Number of days when T_{mean} < 10°C	days	A	5,555
TMlt5	T_{mean} below 5°C	Number of days when T_{mean} < 5°C	days	A	5,555
TMge5	T_{mean} at least 5°C	Number of days when $T_{mean} \geq$ 5°C	days	A	5,556
TMge10	T_{mean} at least 10°C	Number of days when $T_{mean} \geq$ 10°C	days	A	5,556
TX95t[a]	Very warm day threshold	Value of the 95th percentile of T_{max}	°C	H, A	10,214
TXgt50p	Percentage of days with maximum temperature above the median	Percentage of days with T_{max} > 50th percentile	%	H, A, W	4,415
TX*d*TN*d*	User-defined consecutive number of hot days and nights	Annual count of d consecutive days where both T_{max} > 95th per centile and T_{min} > 95th percentile, where $10 \geq d \geq 2$	days	H, A, W	5,765
TXb*d*TNb*d*	User-defined consecutive number of cold days and nights	Annual count of d consecutive days where both T_{max} < 5th per centile and T_{min} < 5th per1centile, where $10 \geq d \geq 2$	days	H, A, W	5,765
Rxdday	Monthly maximum *d*-day precipitation	Maximum rainfall occurring within d consecutive days	mm	H, A, W	8,622
*M*month_SPI[b]	Standardized Precipitation Index	SPI drought measure using precipitation over *M*months		H, A, W	8,767
12month_SPI[b]	Standardized Precipitation Index	SPI drought measure using precipitation over 12 months		H, A, W	9,530

10.1029/2023EA003279

Table 1
Continued

Index	Name	Description	Units	Sector(s)	Stations (1981–2010 ref. Period)
6month_SPI[b]	Standardized Precipitation Index	SPI drought measure using precipitation over 6 months		H, A, W	9,918
3month_SPI[b]	Standardized Precipitation Index	SPI drought measure using precipitation over 3 months		H, A, W	10,026
*M*month_SPEI[b]	Standardized Precipitation Evapotranspiration Index	SPEI drought measure using precipitation and evaporation over *M*months		H, A, W	5,085
12month_SPEI[b]	Standardized Precipitation Evapotranspiration Index	SPEI drought measure using precipitation and evaporation over 12 months		H, A, W	5,787
6month_SPEI[b]	Standardized Precipitation Evapotranspiration Index	SPEI drought measure using precipitation and evaporation over 6 months		H, A, W	6,166
3month_SPEI[b]	Standardized Precipitation Evapotranspiration Index	SPEI drought measure using precipitation and evaporation over 3 months		H, A, W	6,327

Note. The temperatures (*n*) for CDDcold*n*, HDDheat*n* and GDDgrow*n*, consecutive day count (*d*) for CSDI*d*, WSDI*d*, TXdTN*d* and TXbdTNb*d*, and monthly interval (*M*) for SPI and SPEI measures are user defined and discussed in Section 2. The indices labeled in italics are available on a monthly as well as annual basis. The sectors to which the indices are most relevant are listed, using the information as given in the Climpact2 User Guide, Appendix A, where H-Health, A-Agriculture and Food Security, W-Water Resources. This is also available at https://www.climdex.org/learn/indices/sector/. For more details on SPI see McKee et al. (1993), World Meteorological Organisation (2012) and the SPEI see Vicente-Serrano et al. (2010). [a]This index is given as 365 values, one for each day of the year, and so is of a different format to others within the ET-SCI and ETCCDI families. [b]SPI and SPEI indices are available on a monthly basis only.

Table 2
The Various Heat Wave Characteristics Defined by Perkins and Alexander (2013) as Used with the Heat Wave Metrics in Table 3 to Create 20 ET-SCI Indices, For Example, EHF_HWF

Abbreviation	Name	Description	Units	Sector(s)
HWA	Heat wave amplitude	Peak value of the hottest heat wave/coldest cool wave	°C	H, A, W
HWD	Heat wave duration	Length of the longest heat wave in a season as identified by HWN	days	H, A, W
HWF	Heat wave frequency	Sum of the number of days which contribute to heat waves as defined by HWN	days	H, A, W
HWM	Heat wave magnitude	Mean temperature of all heat waves identified by HWN	°C	H, A, W
HWN	Heat wave number	Number of individual heat waves each summer season (November–March in southern hemisphere and May–September in northern hemisphere)	–	H, A, W

Note. These can also be used for cold waves. A heatwave is defined as being at least 3 days long, using the metrics from Table 3. The sectors to which the indices are most relevant are listed, using the information as given in the Climpact2 User Guide, Appendix A, where H-Health, A-Agriculture and Food Security, W-Water Resources. This is also available at https://www.climdex.org/learn/indices/sector/.

The combined set of the Climpact indices (those defined by both the ETCCDI and ET-SCI) now contains over 80 different indices, with a wide range of applications and uses, from the monitoring of climatologically extreme events and conditions, understanding how these events may change in future climates, through to sectoral-specific applications. We also note that many other indices have been created and are being applied across a wide range of studies involving climate and weather information. For our purpose of creating a global perspective of these indices, we have included all of those defined by the ET-SCI in order to allow the intercomparison of all without any specific application in mind. However, it is important that users of these indices do reflect on which are most relevant for their use case and select (combinations of) those which best address their needs.

3. Data

Where possible we have used the same input data as for the HadEX3 data set. These come from a range of sources, including well known international collections (e.g., ECA + D, Klein Tank et al., 2002; Klok & Klein Tank, 2009) and also national sources from individual submissions. For more details on these data sources, see Dunn et al. (2020).

These data have been provided for inclusion in two forms. Some have been provided as daily observations of maximum and minimum temperature, and daily precipitation accumulations. The indices are calculated from these using the Climpact2 v1.3 software (Alexander & Herold, 2015; Herold & Alexander, 2016), written in *R* (Ihaka & Gentleman, 1996; R Core Team, 2013), to match the approach used for the ETCCDI indices in the HadEX3 data set.

Other data have been provided already in the form of pre-calculated indices, which limited the choice of user-defined values as noted above. In many cases these have come from workshops organized by the WMO, where participants were able to process their daily observations into these indices, using the previously mentioned

Table 3
The Various Heat (and Cold) Wave Metrics Used With the Heat Wave Characteristics in Table 2 to Create 20 ET-SCI Indices, For Example, EHF_HWF, TX90_HWA

Heat/Cold wave definition	Name	Heat/cold wave criteria	Units	Sector(s)
ECF	Excess Cold Factor	A cold wave occurs when at least 3 or more days have positive ECF	$°C^2$	H, A, W
EHF	Excess Heat Factor	A heat wave occurs when at least 3 or more days have positive EHF	$°C^2$	H, A, W
TN90		A heat wave occurs when at least 3 or more days have T_{min} > 90th percentile		H, A, W
TX90		A heat wave occurs when at least 3 or more days have T_{max} > 90th percentile		H, A, W

Note. The ECF and EHF metrics are defined in from Nairn and Fawcett (2015), Perkins and Alexander (2013). The percentiles are calculated over the 1981–2010 period. Note that TN90 and TX90 are not the same as the TN90p and TX90p indices from the ETCCDI set. The sectors to which the indices are most relevant are listed, using the information as given in the Climpact2 User Guide, Appendix A, where H-Health, A-Agriculture and Food Security, W-Water Resources. This is also available at https://www.climdex.org/learn/indices/sector/.

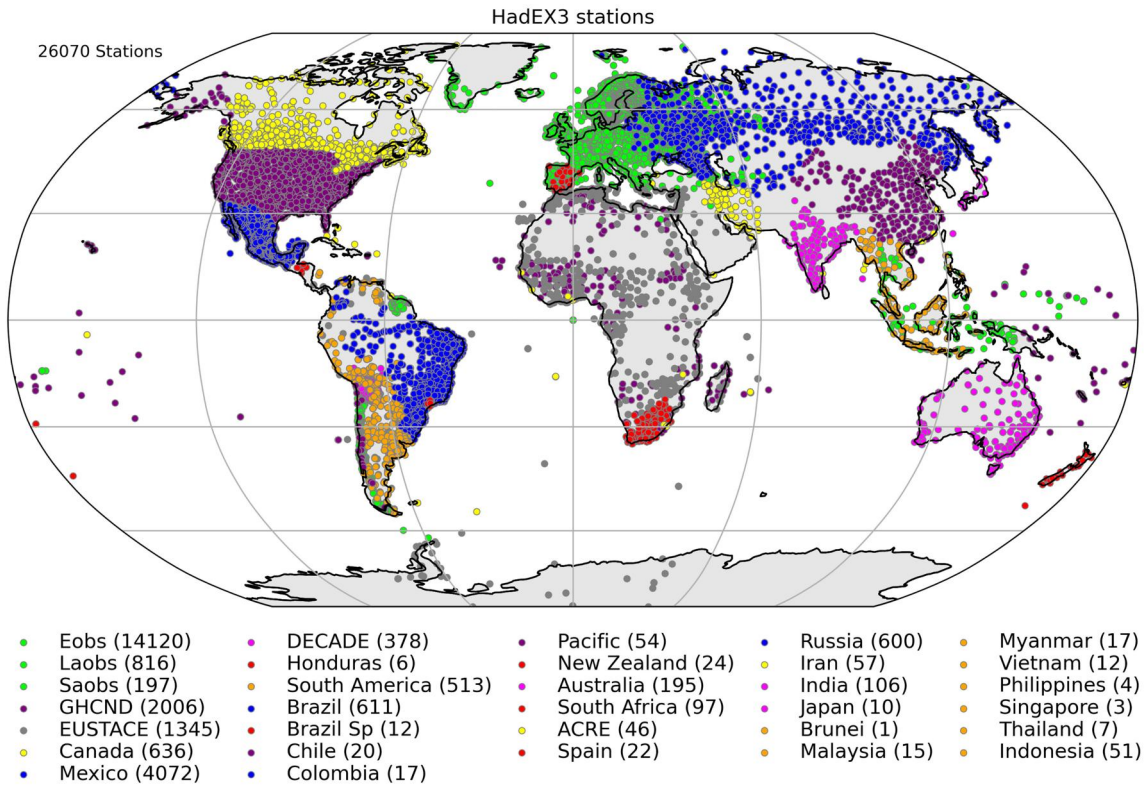

Figure 1. Locations of all stations supplied and available for the sector-specific extension to HadEX3 with a record spanning at least 20 years. Only those ending in 2009 or later and having data gaps of maximum 10 years were selected to form the final grids, with the final numbers of stations varying for each index (see Table 1).

Climpact R-package to ensure consistent calculation. However, not all pre-calculated index data submitted to HadEX3 contained the additional indices defined by the ET-SCI, and there were clear gaps in early development versions of this data set over China and Africa.

We have supplemented the HadEX3 data with daily data from the Global Historical Climate Network Daily data set (GHCNd, Menne et al., 2012) for these two regions, with the greatest effect over China. We perform a detailed comparison of this data set (using GHCNd) and the original HadEX3 (using stations as detailed in Xu et al. (2013)) in Section 5 to highlight any impacts of this change in data source over this region.

We also sourced additional temperature data from stations in Africa and South America from the EUSTACE global station data set (Brugnara et al., 2019; Rayner et al., 2020). Of the 1345 stations available, between around 200 and 300 had long enough records and passed the quality control (QC) checks such that they were included in the final data set, depending on the index. All stations submitted for this extension are shown in Figure 1.

As in the set of indices defined by the ETCCDI, some of the ET-SCI ones also use a reference period to calculate thresholds, but the majority do not. Only CSDI*d*, WSDI*d*, TX*d*TN*d*, TXb*d*TNb*d*, TXgt50p, SPI, SPEI and the heat wave indices are dependent on the choice of a reference period in their construction. In most cases there are more stations available using the 1981–2010 reference period than using 1961–1990, as data from some stations included have records starting in the 1970s. So we use 1981–2010 as our primary reference period. However, as a result of the gridding and interpolation method (see Section 4) this does not immediately translate into greater spatial coverage. We also use 1981–2010 when calculating anomalies for the resulting global timeseries (Section 6).

To match the approach of HadEX3, for these indices only we also provide versions using 1961–1990 as a reference period, as intercomparisons between reference periods for some indices can result in differing trend estimates (Dunn & Morice, 2022).

Table 4
The QC Tests and Which Indices They Have Been Applied to

QC test	Description	Indices
File Checks	Final check for presence of data	All[a]
World Record Check[b]	Exceedance of world record values	TXm, TNm, TMm
Reference period coverage	At least 21 good years during reference period (70% temporal completeness)	All heat wave indices based on TN90 and TX90 thresholds, TXgt50p
Annual in Monthly	Annual value should be one of the monthly ones	Rx*d*day
Annual sum Monthly	Annual value should be sum of the monthly ones	TMge10, TMge5, TMlt10, TMlt5, TNlt2, TNltm2, TXge30, TXge35
Negative Values	No values < 0	All except TXm, TNm, TMm, SPI, SPEI, *_HWA, *_HWM
Consistency	Value of one index to be larger than the [other]	TXm [TMm], TMm [TNm], TMge5 [TMge10], TMlt10 [TMlt5], TXge30 [TXge35], TNlt2 [TNltm2], TNltm2 [TNltm20]
Metadata	Exact matches of latitude and longitude	All
Correlation	High correlation at large distance	TMge10, TMge5, TMlt10, TMlt5, TNlt2, TNltm2, TXge30, TXge35

[a]This test is redundant, but is retained for completeness as in HadEX3. [b]As this is a historical data set, we can use this test. For an updating data set then any flags set by this test would need to be checked manually.

4. Method

We have followed the same approach and steps as for the HadEX3 data set, outlined in Dunn et al. (2020). All the software has been written in Python 3 (Python Software Foundation, 2013), except for Climpact2. The dependencies and interplay between the scripts have been controlled using a Rose (Shin et al., 2019)/Cylc suite (Oliver et al., 2018).

Additional to the HadEX3 data processing, we perform some additional quality control checks on the daily temperature and precipitation observations. Temperature values have to fall within the range of the global records available at the WMO World Weather Archive (https://wmo.asu.edu/). The daily maximum and minimum temperature values have to be consistent with each other (removing values where T_{max} is smaller than T_{min}), and we remove instances where an entire month (where a month of observations must contain at least 10 daily values) has the same value. Precipitation values also have to fall between zero and the highest daily value recorded according to the WMO World Weather Archive.

After calculating the indices (where necessary), and selecting the stations for length of record (at least 20 years of data in the 20th Century, with the last observation occurring in 2009 or later), they are passed through the same QC checks implemented for HadEX3. We show in Table 4 which of those tests are applied to these indices. If values from a station are flagged by any one of the checks, the entire station is withheld from further processing.

Once the QC tests have been completed, we use the Angular Distance Weighting (ADW) method (Shepard, 1968) to interpolate these stations onto a global 1.875° × 1.25° longitude-latitude grid. This method uses a search radius out from the grid box center to identify those stations which will be combined for the final grid box values. The search radius is defined from the decorrelation length scale (DLS), which is determined from the exponential decay curve of the correlation values between all station pairs within 30° latitude bands (60° for the southern hemisphere from 90°S to 30°S) for each index (and month for the monthly indices). The values of the DLS are restricted to between 200 and 2,000 km. The final values for the grid box are the distance-weighted average of the stations which fall within a DLS of the grid box center. At least three stations with valid data need to be present within the DLS for a value to be calculated for a grid box at that time step, with a missing data indicator placed if there are fewer. This ensures that stations with so far unidentified data issues do not overly influence the final grids in regions with few stations. For more details on these steps see Dunn et al. (2020), Donat et al. (2013a, 2013b), Alexander et al. (2006).

As noted in, for example, Dunn et al. (2020, 2022), Avila et al. (2015), the ADW method does have a number of issues, including over-smoothing and interpolation across climate zones when the DLS is large, and the inability to include co-variates like altitude or distance from the coast. However, for consistency with the current HadEX3, we retain the use of ADW for these indices.

4.1. Processing Undefined Values in Heat Wave Indices

A number of the heat wave indices (*_HWA, *_HWD, and *_HWM) are marked by Climpact2 as undefined if no heat wave events were identified for that station in a given year. This is a different case to the values for these indices being missing due to missing data. For example, if a grid cell has no HWA assigned because no heat wave events occurred (not because there were missing data) then this grid cell should not have values from nearby stations interpolated into it, as this would effectively be assigning a heat wave amplitude value where station data shows there were no heat waves. Using a missing data indicator (MDI) would lose valuable information about the behavior of these indices, as the absence of heat wave events is also important to be able to quantify. However, the Climpact2 software does not distinguish between these two cases, using "NA" in both instances. Similarly for *_HWN and *_HWF, "0" (zero) is used when no heatwave occurred and also when the index could not be calculated due to missing daily data. For the heat wave indices only, we perform additional steps to account for these undefined values.

We use the values of other indices to help distinguish whether an "NA" or "0" value arises because the index is undefined or if there are insufficient data points for the index to be calculated and hence should be represented by a MDI (herein −99.9). To determine if the values are truly missing, for the heat wave indices based on the 90th percentile of the maximum temperatures (TX90_*) we use TXx, and for those using minimum temperatures (TN90_*) we use TNn. And for the indices using the ECF and EHF to determine thresholds, we combine both TXx and TNn as both ECF and EHF are based on the mean temperature (which is derived using an average of T_{max} and T_{min}).

As an example for the indices based on TX90, if a year has "NA" for TX90_HWA, TX90_HWD and TX90_HWM and "0" for TX90_HWN and TX90_HWF and is also missing in TXx, then we set that year as missing in the heat wave index using an MDI. However, if there is a value for TXx, then we set that index as undefined using another special value (undefined value indicator, UVI, herein −88.8) for those indices with "NA" set and leave the "0" for TX90_HWN and TX90_HWF. In the data processing steps, the UVIs are masked when calculating the DLS. But they are not handled as missing data when performing the station selection.

In the ADW gridding scheme we have implemented an extra step to handle the undefined values in these heat wave indices. In an approach analogous to the "wet/dry" binary gridding used by Durre et al. (2022), we construct a separate binary field, with 0 in grid boxes with valid index values, and 1 in those with a UVI. The ADW scheme is applied to this field which is then used to mask the gridded values. Locations where this mask is >0.5 are where it is more likely that the index is undefined, and so values in these boxes are replaced with a UVI. Locations where this mask is ≤0.5 are left unmodified.

For the purposes of calculating time series, trends or differences in the HWA, HWD, and HWM metrics, the UVI is replaced by a missing value indicator. These extra undefined values reduce the number of years available for a given grid box, and overall, the temporal completeness requirement (90% of years with values) is much less likely to be met. We therefore do not show the "90%tc" version of this data set (with the temporal completeness restriction) on the time series plots for these indices. These indices are also undefined in the reanalyses data sets when no heat wave occurs, and are represented by missing data indicators. Hence, for this subset of the heat wave indices (shown in Figure 4 and Figures S21–S40 in Supporting Information S1), there is an extra uncertainty arising because of the way these undefined values have been treated as missing in these final steps. In the data files, these values are presented using the UVI.

5. Validation of Data Over China

This sector-specific extension to HadEX3 uses data from a different source over China (228 stations available in the complete GHCND, of which 208 have records of at least 20 years) compared to the HadEX3 data set (319 as detailed in Xu et al. (2013)), as indices from the original source were not available for inclusion. Therefore, we show in Figure 2 comparison time series against the original HadEX3 for three ETCCDI indices (listed in Table 5) covering a range of input measurements and index styles. We use area averages for a region covering from latitude 17°N to 54°N, and longitude 70°E to 135°E, following the approach in Dunn et al. (2020) to demonstrate that there have been no significant differences introduced by the inclusion of this alternative data source.

For TX90p (warm days) there are only very minor differences in this regionally-averaged annual time series, with the largest differences occurring around the late 1940s and early 1950s. TNn (coldest annual temperature) shows

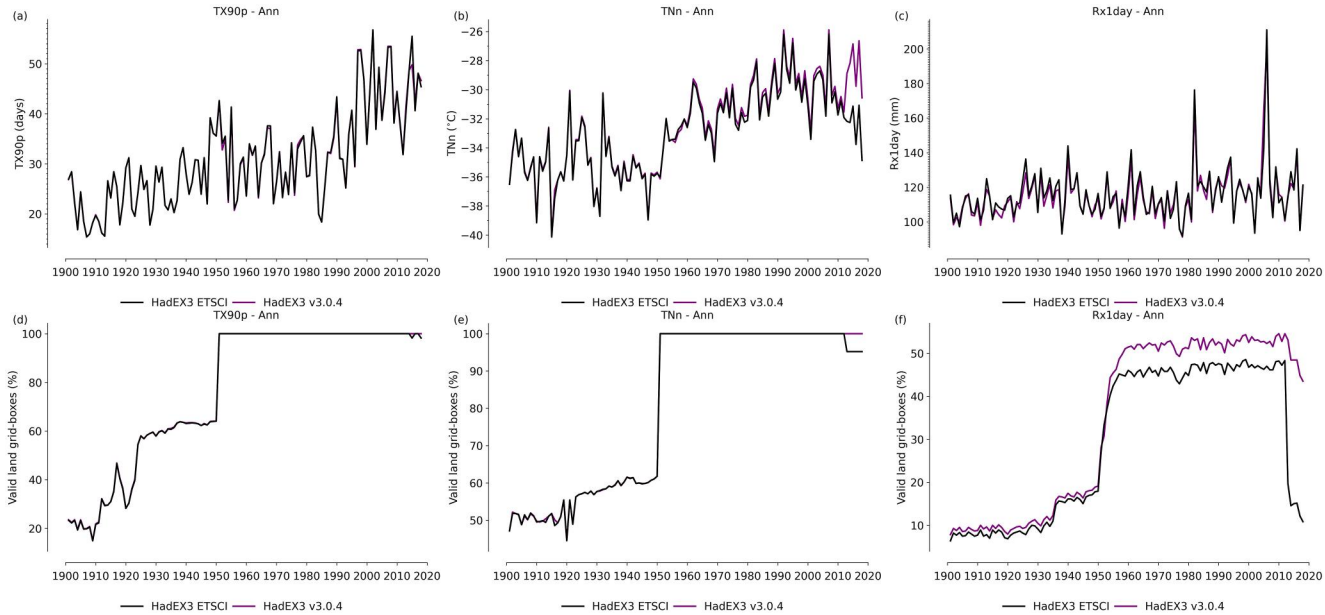

Figure 2. Time series for the area-average of the annual versions of three representative indices (a) TX90p, (b) TNn, and (c) Rx1day. The comparison between the time series demonstrates the impact of the change to using GHCND data over China in this sector-specific extension to HadEX3 from the original HadEX3 (v3.0.4) which used data from the Chinese Meteorological Agency (see Dunn et al. (2020) for details). These indices were calculated purely to enable this comparison, and do not form part of the sector-specific extension. (d–f) Also shown is the fraction of valid land grid boxes in each year for this region for both based data sets.

greater differences than TX90p, especially after around 2010 when the coverage of the selected region is not complete in the new data set. Rx1day (maximum one day precipitation) shows more consistent but still small differences in the regional average throughout the period of record, despite a substantial decrease in the area covered in this new data set (only long-term grid boxes are included in the calculation of the area-average time series). A reduced station number will result in some grid boxes no longer having sufficient stations from which to calculate a value, and hence there is lower coverage when using GHCND in this data set than compared to HadEX3-v3.0.4 for Rx1day. Hence the coverage of precipitation indices in the ET-SCI collection may also be reduced in this part of the world in the final years of the data set when compared to indices in HadEX3-v3.0.4.

However, the use of the GHCND data set to provide in situ data over China does result in very similar behavior compared to the original HadEX3 data set (on an annual basis for these indices over this region). We therefore have included GHCND as an additional data source to ensure that there are some stations from China incorporated into this extension to HadEX3.

6. Global Behavior of the Sector-Specific Indices

The Climpact indices include both those defined by the ETCCDI, which had an initial climatological focus, and those recommended by the ET-SCI which expanded the set to be more sector applicable (see applications in e.g. Herold et al. (2018)). The behavior of the ETCCDI indices was discussed from a climatological point of view in Dunn et al. (2020), and although many of those indices also have applicability to numerous sectors, we do not repeat that discussion here. Hence we will focus on the additional indices recommended by the ET-SCI.

We have followed the same methodology to generate this data set as outlined in Dunn et al. (2020) for HadEX3, and therefore the data set of these indices is also best-suited for the investigation of changes in global or large-regional scales over the last ~120 years. However, studies on local or even grid-box scales are still possible, as long as the blending nature of the ADW is noted; that information and behavior of the indices may have been interpolated from outside of the focus region. The netCDF files include metadata on the number of stations contributing to each grid box which will help in this assessment. Furthermore, this data set provides the global and continental scale context for changes in these indices which can support any regional assessment. For some of the

10.1029/2023EA003279

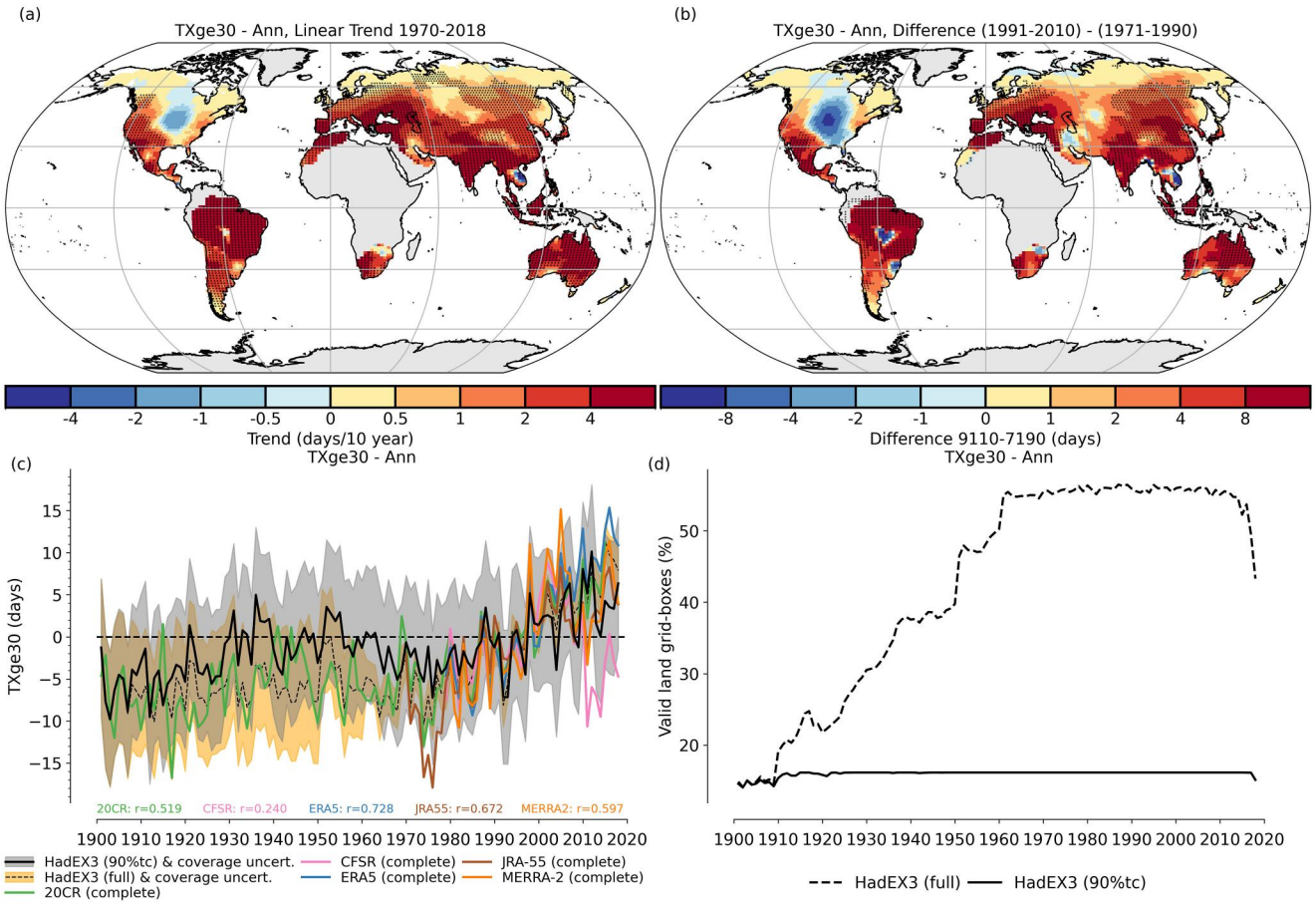

Figure 3. Maps of (a) trends and (b) differences, and time series of the (c) global average anomalies and (d) coverage for annual TXge30 (days, using 1981–2010 as the reference period). Regions shown in white in (a) have values of zero throughout the record, and stippling shows grid boxes where the 95% confidence intervals exclude zero. Stippled regions in (b) are those where a two-sample KS test indicates the distributions are different at a 95% confidence level. In panel (c) along with the time series from the full data set (dotted black line) and grid boxes from the 90% temporally complete subset (90%tc, solid black line), we also show time series from land-masked JRA-55, CFSR, 20CR, ERA5, and MERRA-2 reanalyses, along with their correlation values. In panel (d) we show the coverage of the full data set as well as from the grid boxes which form the 90% temporally complete (90%tc) subset used for the timeseries in (c).

input data sources, indices at the station-level will also be available, allowing site-specific investigations, or generation of higher-resolution, regional data sets.

We also present the behavior of the indices in a similar way to Dunn et al. (2020). In the figures below we show a number of plots for each index. In panel (a) we show the linear trend over 1970–2018, as some station records, especially in South East Asia start in the 1970s. The trend has been calculated using the median of pairwise slopes method (Lanzante, 1996; Sen, 1968; Thiel, 1950). We do not expect changes in these indices to be linear over time, but this is a useful way of displaying the changes. For a trend to be calculated in a grid box, values have to be available for at least 66% of the years (33 years) and the final value of the grid box has to occur in 2009 or later. To give an indication where we can be confident that the trends are not zero, grid boxes where the 95% confidence intervals exclude zero are shown stippled. The spatial coverage over the 1970–2018 period is in most indices relatively constant, apart from the final few years of the record.

We also show these changes in panels (b) which contain the difference between two 20-year averages (1991–2010 minus 1971–1990); this avoids the assumption of a linear trend. The time ranges of these two panels have been defined to optimally reflect the maximum spatial coverage of most of these indices (panels d), as for many indices this is 1970–2010. At least 14 years (66%, rounded up) of data have to be present in each of the two 20-year periods for a difference to be shown, which results in slightly different spatial coverage to the linear trend maps. To give an indication of where we can be confident that these differences are significant, we apply a 2-

10.1029/2023EA003279

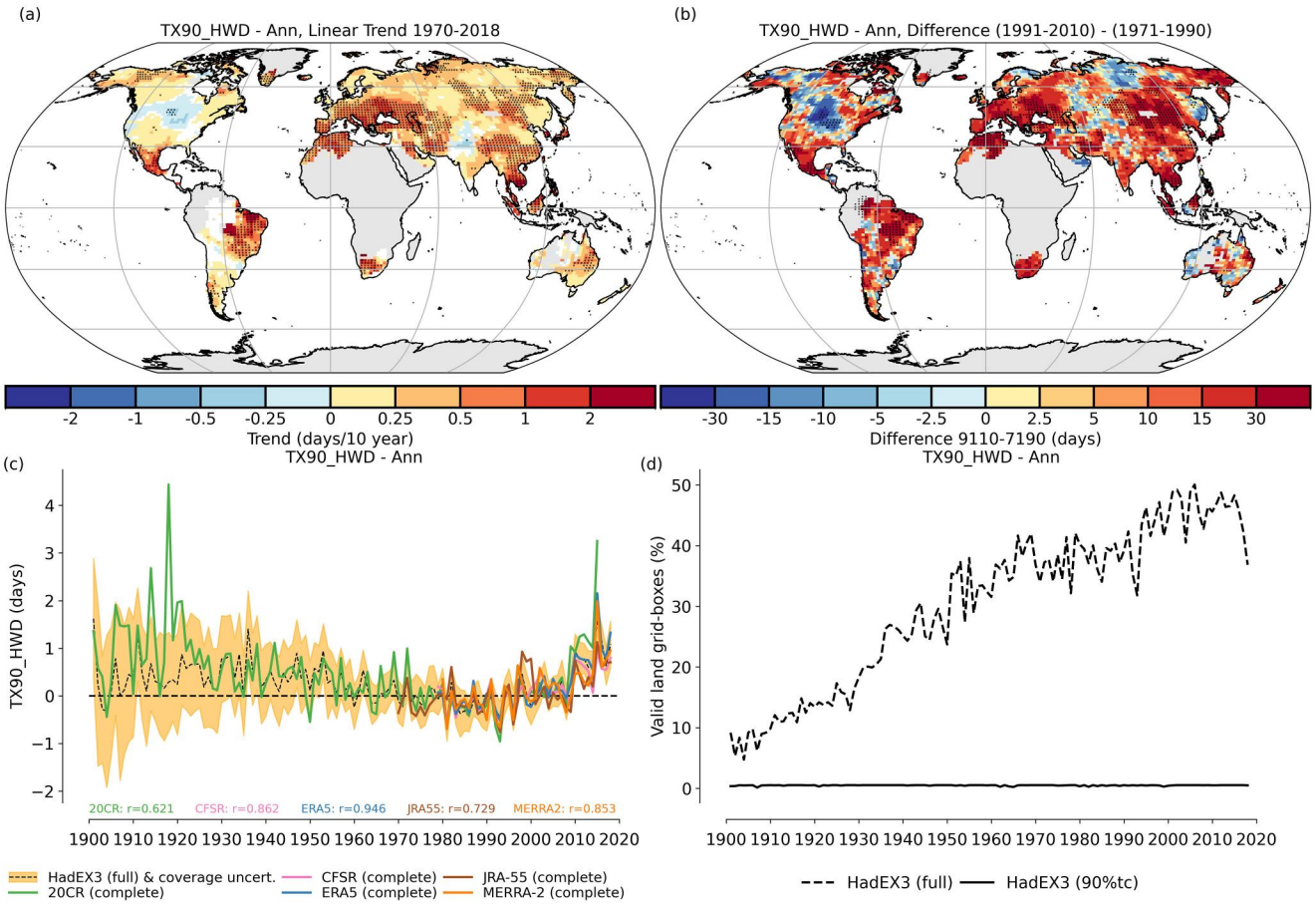

Figure 4. Maps of trends and differences, and time series of the global average and coverage for TX90-HWD (heat wave duration, days), using 1981–2010 as the reference period for the calculation of the 90th percentile. Regions shown in white in (a) have values of zero throughout the record. No time series is calculated using temporally complete grid boxes for this index. No 90% temporal complete version of HadEX3 is shown in (c) because periods where this index is undefined (i.e., no heat waves occurred) mean this criterion is met much less often than for other indices, as shown in panel (d) (see Section 4.1).

sample KS test at a 95% confidence level to the grid boxes. Locations where this indicates the distributions from the two 20-year periods are different are shown with stippling.

In panel (c) we show the "global" land average time series for each index compared to a number of reanalysis products, using anomalies referenced to 1981–2010. We note that there are significant gaps in the spatial coverage of these indices, especially over Africa and parts of South America. Therefore these average time series are first not truly global, and second, they are impacted by the changes in spatial coverage, especially in the early period of this data set. We therefore also show the fraction of land grid boxes with valid data in (d), so that readers can see over which period coverage is relatively stable, and how the early part of the record is affected.

Cosine-latitude weighting has been applied when obtaining the average time series to account for the different grid cell sizes across latitudes. As can be seen from panels (a, b, and d) some indices have large areas of the global

Table 5
The Three "ETCCDI" Indices Used to Validate the Inclusion of a New Data Source Over China

Index	Name	Description	Units
TX90p	Warm days	Percentage of time when daily max temperature ">90th percentile"	%
TNn	Coldest night	Lowest value of daily minimum temperature	°C
Rx1day	Max 1 day precipitation amount	Maximum 1-day precipitation accumulation	mm

land surface without any coverage. We show two versions of the data set, one using all the grid boxes (full) and one which only takes grid boxes which report 90% of the time (90%tc, 106 years out of 118). This latter option has a much smaller spatial coverage (clearly visible in panels (d)), but minimizes the inhomogeneities caused by parts of the world dropping in and out as the underlying station records start and stop.

The coverage uncertainties shown in panel (c) are calculated applying the approach from Brohan et al. (2006) using the ERA5 reanalysis (Hersbach et al., 2019, 2020), as done for the ETCCDI indices in Dunn et al. (2020). The ERA5 data are regridded to match the observations, and for the monthly indices, the appropriate calendar month (e.g., all Januaries) selected. For each year in the reanalysis record, the data are masked by the observational coverage, and a cosine-weighted global average calculated. The residuals between these averages and that from the unmasked reanalysis are obtained. Finally, the standard deviation of the distribution of these residuals is used as an estimate of the coverage uncertainty.

We also show time series for indices calculated for the global land surface from MERRA-2 (Gelaro et al., 2017), JRA-55 (Kobayashi et al., 2015), CFSR (Saha et al., 2010) and 20CR (Slivinski et al., 2019) for comparison, as these reanalyses performed well when compared to the ETCCDI indices in HadEX3 (Dunn et al., 2022). These are using the full land surface, and have not been masked to the spatial coverage of these data. We also include the correlation coefficient of these timeseries of the reanalyses against the 90% temporally complete observational HadEX3 data.

Figures for all indices are shown in Supporting Information S1, along with those referenced to the 1961–1990 reference period.

6.1. Indices Relevant to Health

Exposure to prolonged or extremely low or high temperatures can have severe consequences on physiology. A number of existing ETCCDI indices have clear links to human, animal and plant health, focusing on temperatures above (summer days, SU; tropical nights, TR) or below (frost days, FD; ice days, ID) fixed thresholds, or on duration indices of above or below moderately extreme conditions (warm spell duration index, WSDI and cold spell duration index, CSDI). The new indices which complement these extend the existing indices by adding in higher or lower thresholds for the temperatures, with TXge30 and TXge35 extending SU ("TXgt25") and TNlt2, TNltm2 and TNltm20 extending FD ("TNlt0"). Greater flexibility has been added to the duration indices which now include user-defined versions (WSDI*d* and CSDI*d*).

Other indices which provide new capabilities to monitor changes relevant to heat health are the degree-day measures, with HDDheat*n* and CDDcold*n* measuring the demand for heating or cooling buildings to maintain suitable temperatures. There are also the TX*d*TN*d* and TXb*d*TNb*d* indices which count the number of consecutive hot or cold days and nights. Finally, there are the new heat wave indices, which characterize heat waves and cold waves by their number (of events), frequency (day count), duration (of the longest event), magnitude (mean temperature) and amplitude (peak value reached). These use either the excess heat factor (EHF) or the 90th percentile of the maximum or minimum temperatures to identify heat waves.

We show two examples of these indices, focusing on heat wave events, TXge30 in Figure 3 and TX90_HWD in Figure 4, with figures for all indices being available in Supporting Information S1.

In Figure 3c, it is clear that global values of TXge30 increase from the middle of the 20th Century. The rate of change on a global scale in this data set is smaller than that from the reanalyses data sets, which is likely the result of the lack of information over Africa in the observational product. As can be seen from Figure 3d, although the spatial coverage of the full data set rises to over 50% of land grid boxes, when selecting grid boxes with 90% temporal completeness (90%tc) for the time series shown in Figure 3c, this value is much lower, under 20%. The area available using the 90%tc is determined by 12 years with lowest coverage, usually at the very beginning of the record. The consequence of this is that the "global" average time series from the 90%tc is not representative of the global land area. As noted above, we show this to mitigate the effects of inhomogeneities from varying spatial coverage, but also show the time series of the full data set as well.

The warmer climates in the tropics can result in a more rapid increase in the values of this index than locations in the high latitudes (Figure 3a), as the peak in the distribution of daily maximum temperatures will be closer to the

threshold, and so small increases in the mean result in many more exceedances. However, in areas where the majority of days have maximum temperatures exceeding 30°C, the behavior of this index is more accurately measuring changes in the numbers of "cooler" days, than increases in extremely hot days. And where rainfall is the dominant driver for days to have maximums under 30°C, there is also a link to changes in precipitation patterns.

Of the five reanalyses, four show positive correlations against the 90% temporally complete HadEX3 for TXge30, but only ERA5 has a value $r > 0.7$. The behavior of CFSR after 2010 (see Figure 3c) was also noted in Dunn et al. (2022) for the TNx and TXx indices. But this step-change, which drives the negative correlation value for CFSR, was not seen for TXn and TNn, suggesting that only the warmer values are affected.

There are some regions of decreases in TXge30, which are clearest in for example, in eastern North America, central South America and eastern Southeast Asia (Figure 3b). For South America and Southeast Asia, these decreasing trends can result from artifacts of the gridding process combined with the changing station network in these regions. Values in early years can be interpolated through the ADW method from stations comparatively distant from these locations. When more local stations become available in later years (from 1979 in Southeast Asia) these are more representative of the local climate, and in some cases can result in an apparent anomalous trend, as discussed in Dunn et al. (2022). However, the decreasing trends over North America are over a wide, well-observed region are considered robust and have been called a "warming hole," and a number of explanations have been put forward for this feature (which were also noted in HadEX3 (Dunn et al., 2020)), for example, internal variability (Meehl et al., 2012), land use change (Portmann et al., 2009), and changes in the local hydrological cycle (Eischeid et al., 2023; Pan et al., 2004).

The behavior of the heat wave duration index based on TX90 (TX90_HWD, Figure 4) is more heterogenous than TXge30 shown in Figure 3. This index measures the length of the longest heat wave in a season, where heat waves are identified by at least three days of temperatures above the 90th percentile (defined for each calendar day). In this index if no heat waves were identified for that season, the value of this index is undefined (see Section 4.1). These undefined regions are set to missing when plotting the trend and difference maps and the time series in Figure 4. Also, as noted above, these periods when no heat waves were detected reduce the temporal completeness of each grid box, and also the reanalyses, when calculating the time series for the long-term grid boxes (see limited coverage for 90%tc in Figure 4d). So in Figure 4c we only show the results for the full coverage of the data set.

All reanalyses show clear positive correlations, with CFSR, ERA5, and MERRA-2 having values $r > 0.85$. The time span of 20CR covers the entire period, and shows greater interannual variability in the earlier period, where in situ data for both HadEX3 and 20CR are sparser. The agreement between HadEX3 and all the reanalyses from ~1980 onwards is very good.

The overall pattern of change across the globe is much less uniform than for TXge30, though increases in the duration of the longest heat wave have occurred in many parts of the globe. The behavior seen over the complete record also shows good agreement with the reanalyses. The slow apparent decrease in TX90_HWD since the start of the record toward around 1990, which is also shown by 20CR, occurs as the spatial coverage also increases. The coverage uncertainty encompasses zero change during this time, hence it is unclear whether the initial gradual decrease can be considered to be realistic from a global perspective, due to the relatively low spatial coverage in the first half of the time series, although it is supported by the globally-complete 20CR reanalysis. The non-linear nature of the time series since 1970 (Figure 4c) results in the striking disparity between panels (a) and (b).

This set of ET-SCI indices incorporate a large number of individual indices to capture a range of heat wave characteristics, using the four different metrics to identify heat wave events (see discussion around Tables 2 and 3). For the detailed study of the impacts of changes in heat waves on human, animal and plant health, all these as well as other indices in the Climpact set could be incorporated and compared to other data sets to for example, explore adaptation strategies.

6.2. Indices Relevant to Agriculture and Food Security

A number of the indices relevant to health are also relevant to agriculture and food security, especially considering animal husbandry. However, plant species also have threshold temperatures above/below which they suffer damage or do not grow, set seed and/or fruit. In fact, instantaneous exposure to very high or low temperatures are sufficient for impacts, and so the TXx and TNn indices are included alongside measures

using the daily mean temperature (TMlt5, TMge5, TMlt10, TMge10). Another clearly relevant index is GDDgrow*n* (Growing Degree Days) which complements Growing Season Length (GSL). And of course precipitation indices are also important for agriculture, with the Standardized Precipitation Index (SPI) and Standardized Precipitation Evapotranspiration Index (SPEI) available as standard on a 3, 6, and 12 month accumulation as well as a user-defined timescale (24 months in this extension). Some of these temperature indices use fixed thresholds which may be relevant to certain species. GDDgrow*n* can be tailored to any number of species (both plant and pest) depending on the need of the user. In this global study we have used 10°C, which is relevant for for example, rice, soy and coffee, but also allows for the greatest spatial coverage from the data provided for this global data set.

Multiple indices can also be assessed together (Villa-Falfán et al., 2023) or combined using multiple linear regression models (McGree et al., 2020) to understand the drivers on crop yields, especially in locations where the daily temperature and precipitation data are not freely available for this kind of analysis but this space-filling representation is.

The SPEI is a measure of drought based on precipitation and evapotranspiration measures (Vicente-Serrano et al., 2010), extending the SPI by including temperature information. The Hargreaves method was used to calculate potential evapotranspiration (Hargreaves, 1994; Hargreaves & Allen, 2003; Hargreaves & Samani, 1985). The inclusion of evapotranspiration can be extremely important as any changes in precipitation can be offset or exacerbated by changes in evapotranspiration. Negative values for the SPEI (and SPI) indicate conditions are drier than the 1981–2010 baseline, while positive values indicate wetter conditions. We compared the SPEI values obtained from the daily observations in this study to those derived from monthly observations used by Spinoni et al. (2019). Their Figure 2 shows the 3-month SPEI measure in August 2015, the month with the largest area in drought conditions between 1951 and 2016, and in Figure 5 we show the field for the same month. Large scale patterns of areas under drought qualitatively match well, with central and eastern Europe, eastern Asia and north-western North America all showing SPEI values of less than -1.

Strong long term global changes in 12-month SPEI are not apparent (Figure 6), with the coverage uncertainty of the time series encompassing zero for most of the period of record. There is an increase in SPEI during the middle of the 20th century, coincident with increased spatial coverage, and there are suggestions of a slow drop in global SPEI values from around 1990. However, in Figure 6a there are regions showing consistent changes, with parts of southern Africa, southern Australia, southern South America, and a number of regions around the Mediterranean Sea all showing trends of decreasing 12-month SPEI and hence increasing levels of drought.

The lack of a strong long-term global change also affects the correlations of the reanalyses with the 90% temporally complete HadEX3, as these are dominated by the interannual variation for the 12-month SPEI. The lower spatial coverage in the 90% temporally complete HadEX3 also will affect the representativity of this data set (with only around 10% of global land area being covered), with a smaller fraction of the land area being summarized in the time series, the chances for mismatches with the globally-complete reanalyses are higher.

The global average timeseries of TNltm2 (indicating periods of significant frost, Figure 7) has the opposite pattern to TXge30, with a continual decrease starting around the 1940s. All reanalyses show strong positive correlations with HadEX3, with all but 20CR having $r > 0.9$. Crop fertility can be affected by freezing temperatures and growing seasons can be shifted. The decrease in cold nights is consistent with an overall increase in GSL (Supplemental Figure S10 in Dunn et al. (2020)). Again, there is good agreement between HadEX3 and the reanalysis products (and there is no change in behavior for CFSR post-2010). This index shows a more heterogenous behavior over southern South America, with no large contiguous areas of either increase or decrease. This region is topographically complex, and so the behavior will depend on the locations of the stations in this region. For example, those from the DECADE project (Andrade et al., 2018) come from the central Andes, and many stations are at high altitude (over 2,000 m), whereas those from the LAOBS collection (Van Den Besselaar et al., 2015), from Brazil (from INMET) and from other South American nations (de los Milagros Skansi et al., 2013; Podestá et al., 2013; Veiga et al., 2014) are generally from lower elevations.

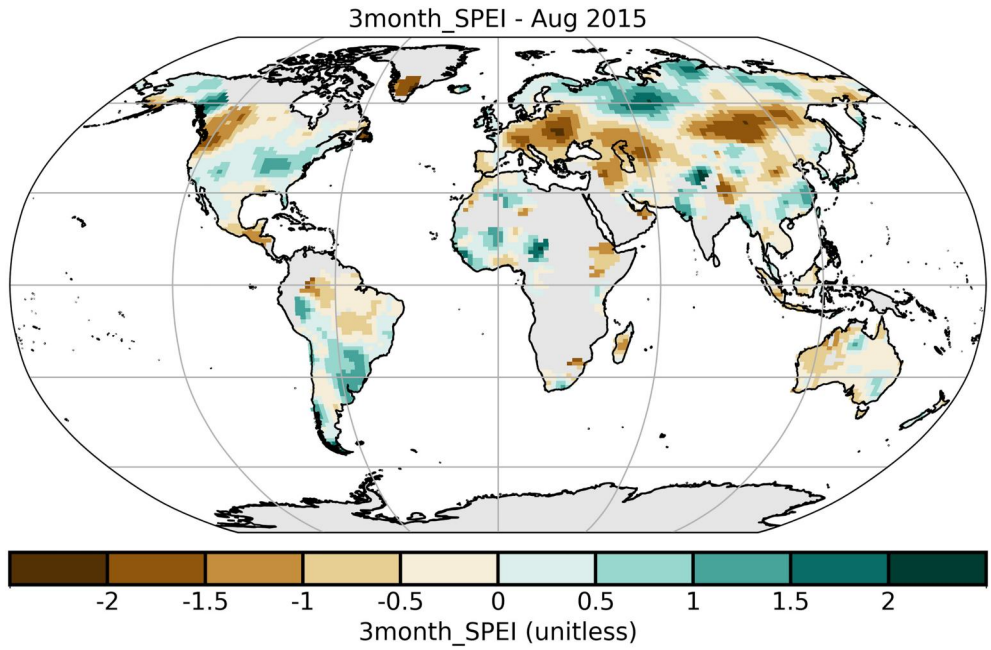

Figure 5. Values of 3-month SPEI for August 2015, the month with the largest area of the globe in drought conditions according to Spinoni et al. (2019). Negative values show regions in drought.

6.3. Indices Relevant to Water Resources

Both too much or too little water pose problems in human societies. The additional ET-SCI indices along with the ones from the ETCCDI collection in the Climpact set predominantly facilitate the study of changes in rainfall characteristics as they are based on daily rainfall accumulations. However, most of the additional indices defined by the ET-SCI are based on daily temperatures, and only a few use the daily precipitation values. SPEI (see above) combines both quantities and is very relevant for water resources since it factors in the evaporative demand of the atmosphere, but the SPI is a measure of drought based solely on the precipitation amounts (McKee et al., 1993), and the 12-month version of the index reflects long-term precipitation patterns (World Meteorological Organisation, 2012). Only some parts of the world show large contiguous areas of consistently changing 12-month SPI where the changes are different from zero (Figures 8a and 8b). And in the global time series there is little evidence for global-scale changes in recent years (Figure 8c). However, there is an increase during the middle of the 20th century, which is coincident with (but not driven by) the progressive increase in spatial coverage between 1940 and 1970 (mainly South America and south-eastern Asia), which leads into the 30 year reference period for the SPI. As the timeseries from the full data set and that from the coverage limited (90%tc) are very similar for the global mean, the coverage unlikely to be the driver for the change in SPI during the 20th century. However, the 20CR shows no strong change in this index over the period, nor do the other reanalyses over their periods.

The indices relevant to water resources are not only those based on precipitation, but also temperature indices that characterize prolonged above average-temperatures for example, TX*d*TN*d*, TXgt50p. These sit alongside the existing ETCCDI precipitation indices which also quantify excess water amounts, such as Rx*d*day which has been introduced here to allow for a user-defined number of days over which to determine a maximum accumulation amount.

7. Summary

We present an extension for a data set that comprises additional sector-specific indices based on daily measurements of precipitation, maximum and minimum temperatures to add to those already well used in the HadEX family of data sets. The addition of these new indices increases the sector-specific applicability of the HadEX3 data product, and is intended to support decision makers in a wide range of sectors with accurate historical information about how the climate is changing.

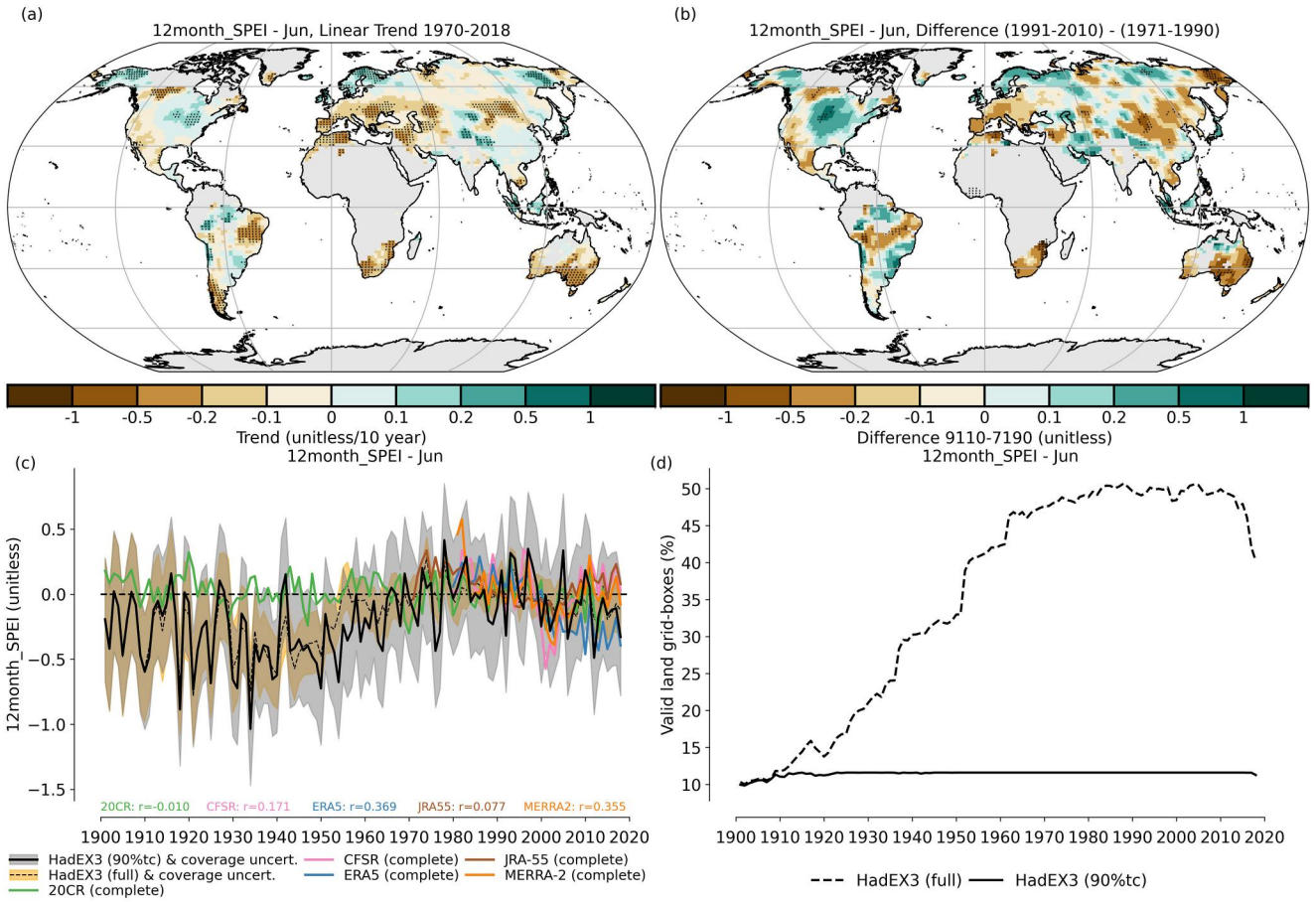

Figure 6. Maps of trends and differences, and time series of the global average anomalies and coverage for annual 12 month-SPEI (using 1981–2010 as the reference period). In panel (d) we show the coverage of the full data set as well as from the grid boxes which form the 90% temporally complete (90%tc) subset used for the timeseries in (c). No annual values for SPEI are calculated, so we show values for June.

To ensure compatibility and continuity, we have performed very similar processing to that used for the HadEX3 data set, and the gridded fields are provided on a 1.875° × 1.25° longitude-latitude grid, covering 1901–2018. This data set has been designed for the study of large scale past changes in these indices, for example, on a global or continental scale.

The issues with the ADW method noted in Dunn et al. (2020, 2022) are also apparent in this data set. Alternative gridding and interpolation methods, which manage the varying station network and incorporate other co-variates, will be necessary for a future version to enable reliable local and regional assessment of changes. On a global and in most cases a continental scale, the current approach does result in good agreement with modern reanalysis products.

Analyses of long-term changes in these indices on a global scale (moderated by limited spatial coverage in e.g. Africa and parts of South America) show increases in the intensity and duration of warm conditions, and corresponding decreases in cool conditions since the middle of the 20th Century. There is good agreement between the direction and magnitude of the changes seen in this product and in globally averaged time series calculated from modern reanalysis products. We note the very poor coverage over Africa for some of these new indices, especially when selecting grid boxes which are 90% temporally complete. The new ET-SCI indices were not always included in the data supplied when constructing the HadEX3, which has limited the spatial coverage. Ongoing efforts in data rescue (e.g., Atmospheric Circulation Reconstructions over the Earth [ACRE, https://www.met-acre.net/], and International Data Rescue [I-DARE, https://www.idare-portal.org/]) and access to in situ records (Noone et al., 2021; Thorne et al., 2017) should also help increase the volume of data available in the

10.1029/2023EA003279

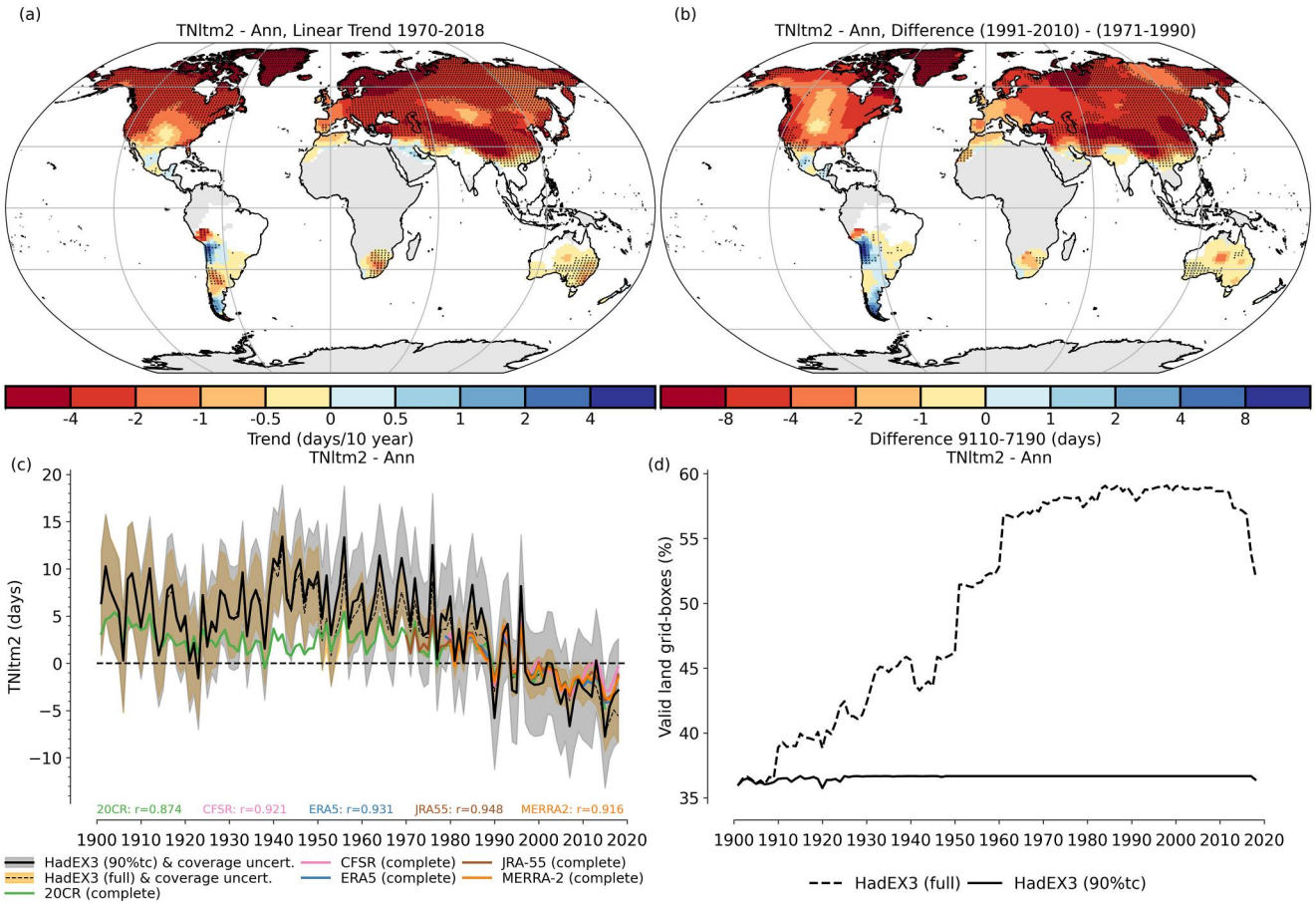

Figure 7. Maps of trends and differences, and time series of the global average anomalies and coverage for annual TNltm2 (using 1981–2010 as the reference period). Regions shown in white in (a, b) have values of zero throughout the record. In panel (d) we show the coverage of the full data set as well as from the grid boxes which form the 90% temporally complete (90%tc) subset used for the timeseries in (c).

future. We have shown herein and also in Dunn et al. (2022) that the reanalyses are often in close agreement with the in situ observation based data sets in regions with good data coverage but large inter-product spread in regions with poor data coverage (e.g., Alexander et al., 2020) mean that caution is required in their interpretation in data sparse regions.

The example indices we have shown indicate that the number of days above 30°C (TXge30) is increasing virtually everywhere, which has potential implications for crop fertility, and freezing days (TNltm2) are decreasing, which can potentially reduce crop damage and change growing seasons. The longest heat waves (TX90_HWD) are getting longer in many regions, which has clear health and energy implications. Droughts are increasing or decreasing depending on the region (12month_SPEI). The Supporting Information S1 contains maps and time series for all the indices and the https://www.climdex.org portal provides a user-friendly interface for exploring and obtaining these data. Decision makers from the health, agriculture and water as well as other sectors are encouraged to explore these resources. These Climpact indices can be combined either together or with other data sets to increase their usefulness and enable the identification of both simple and complex climate risks. The use of these indices in regions where daily temperature and precipitation observations are not available can help with studies in the sectors where these indices are applicable.

The focus of the initial release of HadEX3 (Dunn et al., 2020) was on the indices defined by the ETCCDI, which were amongst the first set developed to allow the study of extremes in a consistent and comparable way for large parts of the globe (Frich et al., 2002; Karl et al., 1999; Peterson, 2005). Additional indices were developed by the ET-SCI to complement the original set, and these two collections combined form the Climpact indices. The new

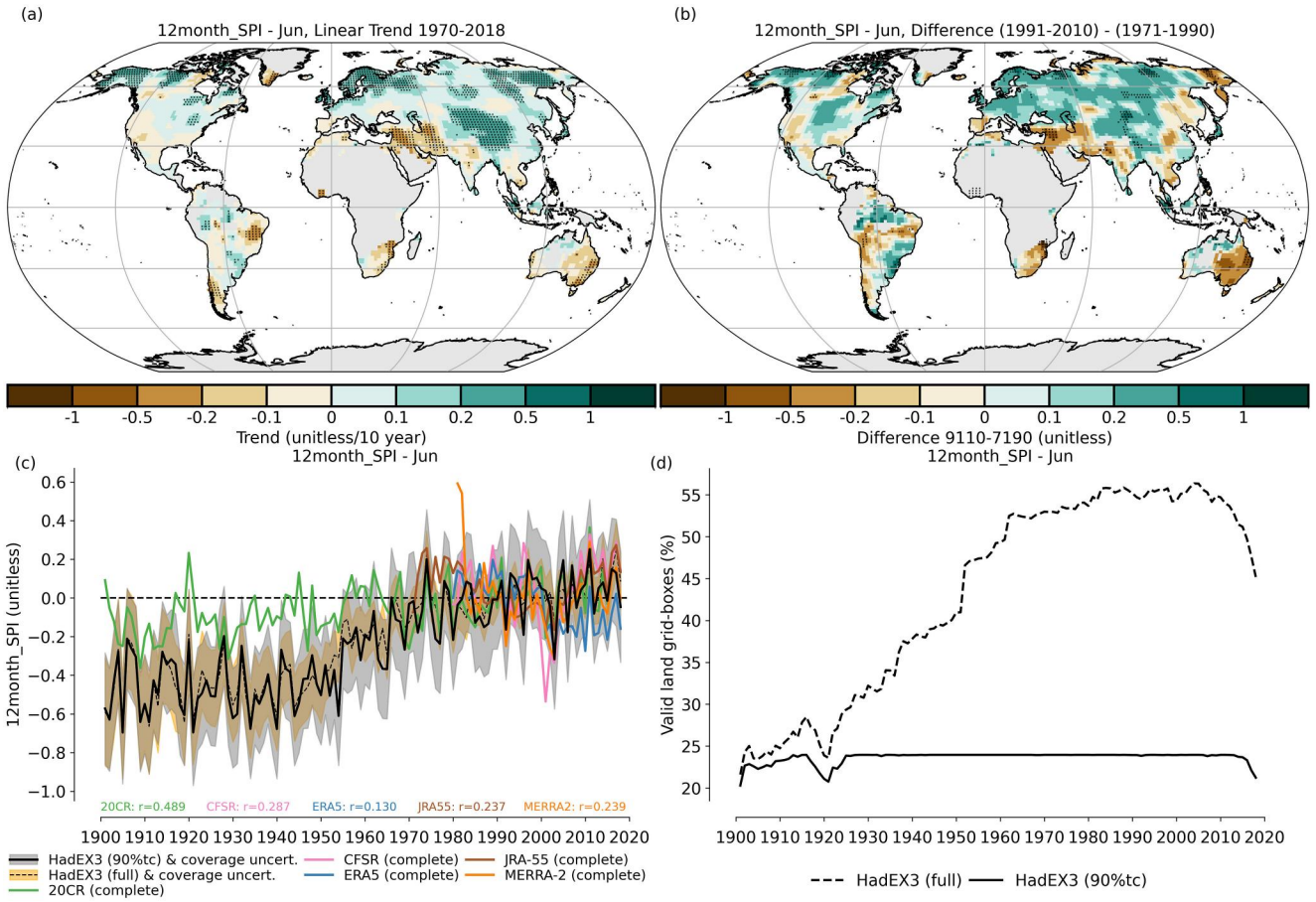

Figure 8. Maps of trends and differences, and time series of the global average anomalies and coverage for annual 12 month-SPI (using 1981–2010 as the reference period). In panel (d) we show the coverage of the full data set as well as from the grid boxes which form the 90% temporally complete (90%tc) subset used for the timeseries in (c). No annual values for SPI are calculated, so we show values for June.

indices that we have included (to give around 80 indices in total) extend the potential uses of the HadEX family of data sets, with a focus on sector specific applications. This now allows users to analyze past changes in extremes from a climatological point of view, as well as investigate these through the lens of certain sectors. Looking forward toward the next update to the HadEX family of data sets, it is likely that all the Climpact indices will be made available contemporaneously.

Indices of concurrent climate extremes—two or more extremes occurring at the same time—are becoming more relevant for adaptation since the frequency of many individual extremes are increasing worldwide (Seneviratne et al., 2021). Hot days and drought from the Climpact indices have been used to assess the changing frequency of hot and dry days (e.g., De Luca & Donat, 2023) and demonstrate more generally how indices of hot/cool and dry/wet days can be combined. Determining the most sector-relevant combination of climate variables and their corresponding thresholds to measure concurrent climate extremes will require ongoing research and the availability of long and high quality sector data (e.g., crop yield or fatalities).

Data Availability Statement

The gridded dataset are available at www.metoffice.gov.uk/hadobs/hadex3 and at www.climdex.org. In addition, a version is available on the CEDA archive (https://dx.doi.org/10.5285/2bfbdba03d9b423f99cadf404ca2daab).

The underlying station indices will be made available on www.climdex.org where we are allowed to do so. For some collections we are not allowed to make the underlying station data public under terms of their licence.

Acknowledgments
All software, with the exception of Climpact2 which is in R (Ihaka & Gentleman, 1996; R Core Team, 2013), have been written in Python 3 (Python Software Foundation, 2013). The dependencies and interplay between them have been controlled using a Rose (Shin et al., 2019)/Cylc suite (Oliver et al., 2018). RJHD was supported by the Met Office Hadley Centre Climate Programme funded by DSIT and by the UK-China Research & Innovation Partnership Fund through the Met Office Climate Science for Service Partnership (CSSP) China under the International Science Partnerships Fund (ISPF), and thanks Kate Willett, Lizzie Good and Nick Rayner for useful discussions and comments. LVA was supported by Australian Research Council Grant CE170100023. MGD is grateful for funding by the Horizon 2020 LANDMARC project (grant agreement no. 869367). JM was supported by the RED-CLIMA (Red Española e Iberoamericana sobre Variabilidad Climática y Servicios Climáticos en Ecosistemas Terrestres y Marinos: RED-CLIMA) Project, under Grant INCCLO0023 from the Consejo Superior de Investigaciones Científicas LINCGLOBAL CSIC from Spain. Additional funding comes from National Institute of Science and Technology for Climate Change Phase 2 under CNPq Grant 465501/2014-1; FAPESP Grant 2014/50848-9; and the National Coordination for Higher Education and Training (CAPES) Grants 88887.136402–00INCT. Data from Southeast Asia (excl. Indonesia) was supported by work on using ClimPACT2 during the Second Workshop on ASEAN Regional Climate Data, Analysis and Projections (ARCDAP-2), 25–29 March 2019, Singapore, jointly funded by Meteorological Service Singapore and WMO through the Canada-Climate Risk and Early Warning Systems (CREWS) initiative. Daily data for Mexico were provided by the Servicio Meteorológico Nacional (SMN) of Comisión Nacional del Agua (CONAGUA). The Pacific data is associated with an ET-SCI workshop in Fiji over 7–11 December 2015 funded by Environment Canada. Additional detail available via https://doi.org/10.1175/JCLI-D-18-0748.1. We acknowledge the data providers in the ECA&D project (http://www.ecad.eu), the SACA&D project (https://sacad.database.bmkg.go.id), and the LACA&D project. We thank Thelma Cinco and Rosaline de Guzman (PAGASA-DOST, Philippines), Imke Durre and Matthew Menne (NOAA-NCEI), Tin Mar Htay (Department of Meteorology and Hydrology, Myanmar), Mahbobeh Khoshkam (I.R. of Iran Meteorological Organization), Gerald Lim and Lim Li-Sha (Meteorological Service Singapore, Singapore), Maria de los Milagros Skansi (Servicio Meteorológico Nacional, Argentina), Chalump Oonariya

References

Alexander, L. V., Bador, M., Roca, R., Contractor, S., Donat, M. G., & Nguyen, P. L. (2020). Intercomparison of annual precipitation indices and extremes over global land areas from in situ, space-based and reanalysis products. *Environmental Research Letters*, *15*(5), 055002. https://doi.org/10.1088/1748-9326/ab79e2

Alexander, L. V., Fowler, H. J., Bador, M., Behrangi, A., Donat, M., Dunn, R., et al. (2019). On the use of indices to study extreme precipitation on sub-daily and daily timescales. *Environmental Research Letters*, *14*(12), 125008. https://doi.org/10.1088/1748-9326/ab51b6

Alexander, L. V., & Herold, N. (2015). Climpactv2 indices and software. A document prepared on behalf of the commission for climatology (CCL) expert team on sector-specific climate indices (ET-SCI).

Alexander, L. V., Zhang, X., Peterson, T. C., Caesar, J., Gleason, B., Klein Tank, A. M. G., et al. (2006). Global observed changes in daily climate extremes of temperature and precipitation. *Journal of Geophysical Research*, *111*(D5), D05109. https://doi.org/10.1029/2005jd006290

Andrade, M. F., Moreno, I., Calle, J., Ticona, L., Blacutt, L., Lavado-Casimiro, W., et al. (2018). Atlas-clima y eventos extremos del altiplano central perú-boliviano. *Geographica Bernensia*. https://doi.org/10.4480/GB2018.N01

Avila, F. B., Dong, S., Menang, K. P., Rajczak, J., Renom, M., Donat, M. G., & Alexander, L. V. (2015). Systematic investigation of gridding-related scaling effects on annual statistics of daily temperature and precipitation maxima: A case study for south-east Australia. *Weather and Climate Extremes*, *9*, 6–16. https://doi.org/10.1016/j.wace.2015.06.003

Brohan, P., Kennedy, J. J., Harris, I., Tett, S. F., & Jones, P. D. (2006). Uncertainty estimates in regional and global observed temperature changes: A new data set from 1850. *Journal of Geophysical Research*, *111*(D12), D12106. https://doi.org/10.1029/2005jd006548

Brugnara, Y., Good, E., Squintu, A. A., van der Schrier, G., & Brönnimann, S. (2019). The Eustace global land station daily air temperature dataset. *Geoscience Data Journal*, *6*(2), 189–204. https://doi.org/10.1002/gdj3.81

de los Milagros Skansi, M., Brunet, M., Sigró, J., Aguilar, E., Groening, J. A. A., Bentancur, O. J., et al. (2013). Warming and wetting signals emerging from analysis of changes in climate extreme indices over south America. *Global and Planetary Change*, *100*, 295–307. https://doi.org/10.1016/j.gloplacha.2012.11.004

De Luca, P., & Donat, M. G. (2023). Projected changes in hot, dry, and compound hot-dry extremes over global land regions. *Geophysical Research Letters*, *50*(13), e2022GL102493. https://doi.org/10.1029/2022GL102493

De Rosa, M., Bianco, V., Scarpa, F., & Tagliafico, L. A. (2014). Heating and cooling building energy demand evaluation; a simplified model and a modified degree days approach. *Applied Energy*, *128*, 217–229. https://doi.org/10.1016/j.apenergy.2014.04.067

Donat, M. G., Alexander, L. V., Yang, H., Durre, I., Vose, R., & Caesar, J. (2013a). Global land-based datasets for monitoring climatic extremes. *Bulletin of the American Meteorological Society*, *94*(7), 997–1006. https://doi.org/10.1175/bams-d-12-00109.1

Donat, M. G., Alexander, L. V., Yang, H., Durre, I., Vose, R., Dunn, R. J. H., et al. (2013b). Updated analyses of temperature and precipitation extreme indices since the beginning of the twentieth century: The HadEX2 dataset. *Journal of Geophysical Research: Atmospheres*, *118*(5), 2098–2118. https://doi.org/10.1002/jgrd.50150

Donat, M. G., Peterson, T., Brunet, M., King, A., Almazroui, M., Kolli, R., et al. (2014). Changes in extreme temperature and precipitation in the Arab region: Long-term trends and variability related to ENSO and NAO. *International Journal of Climatology*, *34*(3), 581–592. https://doi.org/10.1002/joc.3707

Dunn, R. J. H., Alexander, L. V., Donat, M. G., Zhang, X., Bador, M., Herold, N., et al. (2020). Development of an updated global land in situ-based data set of temperature and precipitation extremes: HadEX3. *Journal of Geophysical Research: Atmospheres*, *125*(16), e2019JD032263. https://doi.org/10.1029/2019JD032263

Dunn, R. J. H., Donat, M. G., & Alexander, L. V. (2022). Comparing extremes indices in recent observational and reanalysis products. *Frontiers in Climate*, *4*, 989505. https://doi.org/10.3389/fclim.2022.989505

Dunn, R. J. H., & Morice, C. P. (2022). On the effect of reference periods on trends in percentile-based extreme temperature indices. *Environmental Research Letters*, *17*(3), 034026. https://doi.org/10.1088/1748-9326/ac52c8

Durre, I., Arguez, A., Schreck, C. J., Squires, M. F., & Vose, R. S. (2022). Daily high-resolution temperature and precipitation fields for the contiguous United States from 1951 to present. *Journal of Atmospheric and Oceanic Technology*, *39*(12), 1837–1855. https://doi.org/10.1175/JTECH-D-22-0024.1

Eischeid, J. K., Hoerling, M. P., Quan, X.-W., Kumar, A., Barsugli, J., Labe, Z., et al. (2023). Why has the summertime central U.S. warming hole not disappeared? *Journal of Climate*, *1–49*(20), 7319–7336. https://doi.org/10.1175/JCLI-D-22-0716.1

Ferchault de Réaumur, R. A. (1735). Observations du thermometre, faites a Paris pendant l'annees 1735, comparees a celles qui ont ete faites sous la ligne, a l'isle de France, a alger et en quelques-unes de nos isles de l'amerique. Mémoire de l'Académie royale des sciences. Retrieved from https://www.academie-sciences.fr/pdf/dossiers/Reaumur/Reaumur_pdf/p545_576_vol3532m.pdf

Frich, P., Alexander, L. V., Della-Marta, P., Gleason, B., Haylock, M., Tank, A. K., & Peterson, T. (2002). Observed coherent changes in climatic extremes during the second half of the twentieth century. *Climate Research*, *19*(3), 193–212. https://doi.org/10.3354/cr019193

Gelaro, R., McCarty, W., Suárez, M. J., Todling, R., Molod, A., Takacs, L., et al. (2017). The modern-era retrospective analysis for research and applications, version 2 (MERRA-2). *Journal of Climate*, *30*(14), 5419–5454. https://doi.org/10.1175/jcli-d-16-0758.1

Hargreaves, G. H. (1994). Defining and using reference evapotranspiration. *Journal of Irrigation and Drainage Engineering*, *120*(6), 1132–1139. https://doi.org/10.1061/(asce)0733-9437(1994)120:6(1132)

Hargreaves, G. H., & Allen, R. G. (2003). History and evaluation of Hargreaves evapotranspiration equation. *Journal of Irrigation and Drainage Engineering*, *129*(1), 53–63. https://doi.org/10.1061/(asce)0733-9437(2003)129:1(53)

Hargreaves, G. H., & Samani, Z. A. (1985). Reference crop evapotranspiration from temperature. *Applied Engineering in Agriculture*, *1*(2), 96–99. https://doi.org/10.13031/2013.26773

Herold, N., & Alexander, L. (2016). Climpact 2. Retrieved from https://github.com/ARCCSS-extremes/climpact2

Herold, N., Ekström, M., Kala, J., Goldie, J., & Evans, J. (2018). Australian climate extremes in the 21st century according to a regional climate model ensemble: Implications for health and agriculture. *Weather and Climate Extremes*, *20*, 54–68. https://doi.org/10.1016/j.wace.2018.01.001

Hersbach, H., Bell, B., Berrisford, P., Hirahara, S., Horányi, A., Muñoz-Sabater, J., et al. (2020). The ERA5 global reanalysis. *Quarterly Journal of the Royal Meteorological Society*, *146*(730), 1999–2049. https://doi.org/10.1002/qj.3803

Hersbach, H., Bell, B., Berrisford, P., Horányi, A., Sabater, J., Nicolas, J., et al. (2019). Global reanalysis: Goodbye ERA-Interim, hello ERA5. *ECMWF Newsletter*, *159*, 17–24.

Ihaka, R., & Gentleman, R. (1996). R: A language for data analysis and graphics. *Journal of Computational & Graphical Statistics*, *5*(3), 299–314. https://doi.org/10.2307/1390807

Karl, T. R., Nicholls, N., & Ghazi, A. (1999). CLIVAR/GCOS/WMO workshop on indices and indicators for climate extremes workshop summary. In *Weather and climate extremes* (pp. 3–7). Springer.

and Nichanun Trachow (Thai Meteorological Department, Thailand), Cham Pham (National center for Hydro-Meteorological Forecasting of Vietnam, Vietnam), Fatemeh Rahimzadeh (formerly Atmospheric Science and Meteorological Research Center, Iran), Ernesto Salgado Rubio (Servicio Meteorológico Nacional, Honduras), Ardhasena Sopaheluwakan (Agency for Meteorology Climatology and Geophysics (BMKG), Indonesia), Lucie Vincent (Environment and Climate Change Canada, Canada) for supplying data used in this work. We also thank all those who have supplied data for all the HadEX datasets over the past two decades.

Klein Tank, A. M. G., Wijngaard, J. B., Können, G. P., Böhm, R., Demarée, G., Gocheva, A., et al. (2002). Daily dataset of 20th-century surface air temperature and precipitation series for the European climate assessment. *International Journal of Climatology: A Journal of the Royal Meteorological Society*, *22*(12), 1441–1453. https://doi.org/10.1002/joc.773

Klok, E., & Klein Tank, A. M. G. (2009). Updated and extended European dataset of daily climate observations. *International Journal of Climatology*, *29*(8), 1182–1191. https://doi.org/10.1002/joc.1779

Kobayashi, S., Ota, Y., Harada, Y., Ebita, A., Moriya, M., Onoda, H., et al. (2015). The JRA-55 reanalysis: General specifications and basic characteristics. *Journal of the Meteorological Society of Japanese Series II*, *93*(1), 5–48. https://doi.org/10.2151/jmsj.2015-001

Lanzante, J. R. (1996). Resistant, robust and non-parametric techniques for the analysis of climate data: Theory and examples, including applications to historical radiosonde station data. *International Journal of Climatology: A Journal of the Royal Meteorological Society*, *16*(11), 1197–1226. https://doi.org/10.1002/(sici)1097-0088(199611)16:11<1197::aid-joc89>3.0.co;2-l

McGree, S., Schreider, S., Kuleshov, Y., & Prakash, B. (2020). On the use of mean and extreme climate indices to predict sugar yield in western Fiji. *Weather and Climate Extremes*, *29*, 100271. https://doi.org/10.1016/j.wace.2020.100271

McKee, T. B., Doesken, N. J., & Kleist, J. (1993). The relationship of drought frequency and duration to time scales. In *Proceedings of the 8th conference on applied climatology* (Vol. 17, pp. 179–183).

Meehl, G. A., Arblaster, J. M., & Branstator, G. (2012). Mechanisms contributing to the warming hole and the consequent us east–west differential of heat extremes. *Journal of Climate*, *25*(18), 6394–6408. https://doi.org/10.1175/jcli-d-11-00655.1

Menne, M. J., Durre, I., Vose, R. S., Gleason, B. E., & Houston, T. G. (2012). An overview of the global historical climatology network-daily database. *Journal of Atmospheric and Oceanic Technology*, *29*(7), 897–910. https://doi.org/10.1175/jtech-d-11-00103.1

Meteorological Service Singapore. (2019). Second workshop on ASEAN regional climate data, analysis and projections (ARCDAP-2): Workshop report.

Nairn, J. R., & Fawcett, R. J. (2015). The excess heat factor: A metric for heatwave intensity and its use in classifying heatwave severity. *International Journal of Environmental Research and Public Health*, *12*(1), 227–253. https://doi.org/10.3390/ijerph120100227

Nairn, J. R., Ostendorf, B., & Bi, P. (2018). Performance of excess heat factor severity as a global heatwave health impact index. *International Journal of Environmental Research and Public Health*, *15*(11), 2494. https://doi.org/10.3390/ijerph15112494

Nakaegawa, T., & Murazaki, K. (2022). Historical trends in climate indices relevant to surface air temperature and precipitation in Japan for recent 120 years. *International Journal of Climatology*, *42*(16), 8950–8970. https://doi.org/10.1002/joc.7784

Noone, S., Atkinson, C., Berry, D. I., Dunn, R. J. H., Freeman, E., Perez Gonzalez, I., et al. (2021). Progress towards a holistic land and marine surface meteorological database and a call for additional contributions. *Geoscience Data Journal*, *8*(2), 103–120. https://doi.org/10.1002/gdj3.109

Oliveira, A., Lopes, A., & Soares, A. (2022). Excess heat factor climatology, trends, and exposure across European functional urban areas. *Weather and Climate Extremes*, *36*, 100455. https://doi.org/10.1016/j.wace.2022.100455

Oliver, H. J., Shin, M., & Sanders, O. (2018). Cylc: A workflow engine for cycling systems. *Journal of Open Source Software*, *3*(27), 737. https://doi.org/10.21105/joss.00737

Pan, Z., Arritt, R. W., Takle, E. S., Gutowski, W. J., Jr., Anderson, C. J., & Segal, M. (2004). Altered hydrologic feedback in a warming climate introduces a "warming hole". *Geophysical Research Letters*, *31*(17), 267. https://doi.org/10.1029/2004gl020528

Perkins, S. E., & Alexander, L. V. (2013). On the measurement of heat waves. *Journal of Climate*, *26*(13), 4500–4517. https://doi.org/10.1175/jcli-d-12-00383.1

Peterson, T. C. (2005). Climate change indices. *World Meteorological Organization Bulletin*, *54*(2), 83–86.

Podestá, G., Skansi, M., Herrera, N., Veiga, H., & Rovere, S. (2013). Reporte técnico crc-sas-2013-001: Diseño del proceso de control de calidad de datos climáticos diarios en el centro regional del clima para el sur de américa del sur. Retrieved from http://www.crc-sas.org/es/pdf/reporte_tecnico_CRC-SAS-2013-001.pdf

Portmann, R. W., Solomon, S., & Hegerl, G. C. (2009). Spatial and seasonal patterns in climate change, temperatures, and precipitation across the United States. *Proceedings of the National Academy of Sciences*, *106*(18), 7324–7329. https://doi.org/10.1073/pnas.0808533106

Python Software Foundation. (2013). Python language reference, version 3.6.8. Retrieved from http://www.python.org

Quayle, R. G., & Diaz, H. F. (1980). Heating degree-day data applied to residential heating energy-consumption. *Journal of Applied Climatology*, *19*(3), 241–246. https://doi.org/10.1175/1520-0450(1980)019⟨0241:HDDDAT⟩2.0.CO;2

Rayner, N. A., Auchmann, R., Bessembinder, J., Brönnimann, S., Brugnara, Y., Capponi, F., et al. (2020). The EUSTACE project: Delivering global, daily information on surface air temperature. *Bulletin of the American Meteorological Society*, *101*(11), E1924–E1947. https://doi.org/10.1175/bams-d-19-0095.1

R Core Team. (2013). R: A language and environment for statistical computing [Computer software manual]. *Vienna, Austria*. Retrieved from http://www.R-project.org/

Saha, S., Moorthi, S., Pan, H.-L., Wu, X., Wang, J., Nadiga, S., et al. (2010). The NCEP climate forecast system reanalysis. *Bulletin of the American Meteorological Society*, *91*(8), 1015–1058. https://doi.org/10.1175/2010bams3001.1

Sen, P. K. (1968). Estimates of the regression coefficient based on Kendall's tau. *Journal of the American Statistical Association*, *63*(324), 1379–1389. https://doi.org/10.2307/2285891

Seneviratne, S. I., Zhang, X., Adnan, M., Badi, W., Dereczynski, C., Di Luca, A., et al. (2021). Weather and climate extreme events in a changing climate (chapter 11). In *Climate change 2021: The physical science basis. Contribution of working group I to the sixth assessment report of the intergovernmental panel on climate change*. Cambridge University Press. https://doi.org/10.1017/9781009157896.013

Shepard, D. (1968). A two-dimensional interpolation function for irregularly-spaced data. In *Proceedings of the 1968 23rd ACM national conference* (pp. 517–524).

Shin, M., Fitzpatrick, B., Clark, A., Sanders, O., Bartholomew, S. L., Whitehouse, S., et al. (2019). Rose software. https://doi.org/10.5281/zenodo.3458111

Slivinski, L. C., Compo, G. P., Whitaker, J. S., Sardeshmukh, P. D., Giese, B. S., McColl, C., et al. (2019). Towards a more reliable historical reanalysis: Improvements for version 3 of the twentieth century reanalysis system. *Quarterly Journal of the Royal Meteorological Society*, *145*(724), 2876–2908. https://doi.org/10.1002/qj.3598

Spinoni, J., Barbosa, P., De Jager, A., McCormick, N., Naumann, G., Vogt, J. V., et al. (2019). A new global database of meteorological drought events from 1951 to 2016. *Journal of Hydrology: Regional Studies*, *22*, 100593. https://doi.org/10.1016/j.ejrh.2019.100593

Spinoni, J., Vogt, J. V., Barbosa, P., Dosio, A., McCormick, N., Bigano, A., & Füssel, H.-M. (2018). Changes of heating and cooling degree-days in Europe from 1981 to 2100. *International Journal of Climatology*, *38*(S1), e191–e208. https://doi.org/10.1002/joc.5362

Thiel, H. (1950). A rank-invariant method of linear and polynomial regression analysis, parts 1–3. In *Proceedings of koninalijke nederlandse akademie van weinenschatpen a* (Vol. 53, pp. 386–392).

Thom, E. C. (1959). The discomfort index. *Weatherwise*, *12*(2), 57–61. https://doi.org/10.1080/00431672.1959.9926960

Thom, H. C. S. (1954). The rational relationship between heating degree days and temperature. *Monthly Weather Review*, *82*(1), 1–6. https://doi.org/10.1175/1520-0493(1954)082<0001:trrbhd>2.0.co;2

Thorne, P. W., Allan, R. J., Ashcroft, L., Brohan, P., Dunn, R. J. H., Menne, M. J., et al. (2017). Toward an integrated set of surface meteorological observations for climate science and applications. *Bulletin of the American Meteorological Society*, *98*(12), 2689–2702. https://doi.org/10.1175/bams-d-16-0165.1

Van Den Besselaar, E. J., Klein Tank, A. M., Van Der Schrier, G., Abass, M. S., Baddour, O., Van Engelen, A. F., et al. (2015). International climate assessment & dataset: Climate services across borders. *Bulletin of the American Meteorological Society*, *96*(1), 16–21. https://doi.org/10.1175/bams-d-13-00249.1

Veiga, H., Herrera, N., de los Milagros Skansi, M., & Podestá, G. (2014). *Reporte técnico crc-sas-2014-001: Descripción de controles de calidad de datos climáticos diarios implementados por el centro regional del clima para el sur de américa del sur* (Vol. 2). Centro Regional de Clima para el sur de Amércia del Srur. Retrieved from http://www.crc-sas.org/es/pdf/reporte_tecnico_CRC-SAS-2014-001.pdf

Vicente-Serrano, S. M., Beguería, S., & López-Moreno, J. I. (2010). A multiscalar drought index sensitive to global warming: The standardized precipitation evapotranspiration index. *Journal of Climate*, *23*(7), 1696–1718. https://doi.org/10.1175/2009jcli2909.1

Villa-Falfán, C., Valdés-Rodríguez, O. A., Vázquez-Aguirre, J. L., & Salas-Martínez, F. (2023). Climate indices and their impact on maize yield in Veracruz, Mexico. *Atmosphere*, *14*(5), 778. https://doi.org/10.3390/atmos14050778

Wang, B.-J., Dong, S.-Y., Hu, T., & Sun, Y. (2023). Changes of extreme cold events in China over the last century based on reanalysis data. *Advances in Climate Change Research*, *19*(4), 403–417. https://doi.org/10.12006/j.issn.1673-1719.2022.237

World Meteorological Organisation. (2012). Standardized precipitation index user guide [Computer software manual]. *WMO*. Retrieved from http://www.wamis.org/agm/pubs/SPI/WMO_1090_EN.pdf

Xu, W., Li, Q., Wang, X. L., Yang, S., Cao, L., & Feng, Y. (2013). Homogenization of Chinese daily surface air temperatures and analysis of trends in the extreme temperature indices. *Journal of Geophysical Research: Atmospheres*, *118*(17), 9708–9720. https://doi.org/10.1002/jgrd.50791

Zhang, X., Alexander, L., Hegerl, G. C., Jones, P., Tank, A. K., Peterson, T. C., et al. (2011). Indices for monitoring changes in extremes based on daily temperature and precipitation data. *Wiley Interdisciplinary Reviews: Climate Change*, *2*(6), 851–870. https://doi.org/10.1002/wcc.147